

A Microengineered Brain-Chip to Model Neuroinflammation in Humans

I. Pediaditakis^{1,9†*}, K. R. Kodella^{1,2†}, D. V. Manatakis¹, C. Y. Le¹, S. Barthakur¹, A. Sorets¹, A. Gravanis², L. Ewart¹, L. L. Rubin^{3,4,5}, E. S. Manolakos^{6,7}, C. D. Hinojosa¹, K. Karalis^{1,8,10*}

¹Emulate Inc., 27 Drydock Avenue, Boston, MA 02210, USA.

²University of Crete Medical School, Department of Pharmacology, Heraklion, 71110 Greece.

³Department of Stem Cell and Regenerative Biology, Harvard University, Cambridge, MA, USA.

⁴Harvard Stem Cell Institute, Cambridge, MA, USA.

⁵Broad Institute of Massachusetts Institute of Technology and Harvard, Cambridge, MA, USA.

⁶Department of Informatics and Telecommunications, National and Kapodistrian University of Athens, Greece.

⁷Northeastern University, Bouvé College of Health Sciences, Boston, MA, USA.

⁸Endocrine Division, Children's Hospital, Harvard Medical School, Boston, MA, USA.

⁹Present address: Vesalius Therapeutics Inc., 100 Binney St, Cambridge, MA, 02142, USA

¹⁰Present address: Regeneron Pharmaceuticals, 777 Old Saw Mill River Rd, Tarrytown, NY, 10591, USA

†These authors contributed equally

*Corresponding authors: spediaditakis@vesaliustx.com, katia.karalis@regeneron.com

Keywords: Organs-on-Chip, Neurovascular Unit, Blood-Brain Barrier, Neuroinflammation

SUMMARY

Species differences in the brain and the blood-brain barrier (BBB) biology hamper the translation from animal models to humans and impede the development of specific therapeutics for brain diseases. Here we present a human Brain-Chip engineered to recapitulate critical aspects of the complex brain cell-cell interactions that mediate neuroinflammation development. Our human organotypic microphysiological system (MPS) includes endothelial-like cells, pericytes, glia, and cortical neurons and maintains BBB permeability at *in vivo* relevant levels, providing a significant improvement in complexity and clinical mimicry compared to previous MPS models. This is the first report of a Brain-Chip with an RNA expression profile close to that of the adult human cortex and that demonstrates advantages over Transwell culture. Through perfusion of TNF- α , we recreated key inflammatory features, such as glia activation, the release of proinflammatory cytokines, and increased barrier permeability. Our model may provide a reliable tool for mechanistic studies in neuron-glia interactions and dysregulation of BBB function during neuroinflammation.

47 INTRODUCTION

48 Neurodegenerative diseases (ND) are a serious public health problem, with their
49 increasing burden accounting for more than one billion affected people worldwide (Carroll,
50 2019). Although the molecular mechanisms underlying changes in brain cell-to-cell
51 interactions associated with ND have been elucidated to a significant extent, therapeutic
52 targets and predictive biomarkers are still lacking. Emerging evidence points to
53 inflammation as a major pathogenetic mechanism for neuropathology underlying
54 neurodegenerative diseases (Guzman-Martinez et al., 2019a; Minghetti, 2005). Growing
55 evidence indicates that brain events, such as local ischemia and systemic inflammatory
56 conditions, create a microenvironment favoring the entry of peripheral activated immune
57 cells, or their secreted proinflammatory factors, into the brain by compromising the
58 integrity of the blood-brain barrier (BBB) (Perry et al., 2007a). There is a large body of
59 evidence for a pivotal role of microglia and astrocytes in the pathogenesis of
60 neurodegenerative disorders (Crotti and Ransohoff, 2016; Kim and Joh, 2006; Liddelow
61 and Barres, 2017; Liddelow et al., 2017; Linnerbauer et al., 2020; Perry et al., 2010).
62 Activation of microglia is characterized by the production of cytotoxic molecules and pro-
63 inflammatory cytokines, affecting cellular homeostasis, and ultimately establishing a
64 microenvironment driving neuronal damage (Perry et al., 2010).

65 In addition, reactive astrocytes are also found to be implicated in impaired neuronal
66 function and survival promoting inflammation and increasing cell damage in the CNS
67 (Horng et al., 2017; Liddelow and Barres, 2017; Linnerbauer et al., 2020; Sofroniew,
68 2020). Additional reports suggest a crosstalk between astrocytes and microglia in the
69 context of neuroinflammation and neurodegeneration (Linnerbauer et al., 2020). Reactive
70 microglia and astrocytes are likely to contribute to the leaky BBB observed in these
71 diseases through downregulation of paracellular tight-junction proteins such as Occludin
72 and zonula occludens-1 (ZO-1) (Keaney and Campbell, 2015; Obermeier et al., 2013).

73 Despite the progress in understanding the mechanisms mediating the effects of immune
74 activation in the brain (González et al., 2014), the translation of these findings to effective,
75 specific treatments lags significantly. Species differences between human and the
76 currently used experimental *in vivo* animal models of ND, together with the inherent
77 limitations of the primary brain rodent cells or human cell lines currently used as *in*
78 *vitro* models, are greatly implicated in this problem. Advances in stem cell biology have
79 recently enabled new human cell models for experimentation, such as iPSC-derived brain
80 cells and complex, multi-layered 3D organoids (Bose et al., 2021; Dolmetsch and
81 Geschwind, 2011; Yin et al., 2016). These systems can provide new insights into tissue
82 biology and our understanding of the interindividual differences in brain functions.
83 Exploiting these systems can be significantly advanced by their culture in
84 microphysiological platforms providing a perfusable vascular system and an overall
85 physiologically relevant microenvironment, by enabling long-lasting cell interactions and
86 the associated functionality (Cucullo et al., 2011). Recent reports describe applications of
87 this technology in developing Organ-Chips that recapitulate aspects of the complex BBB
88 functions (Ahn et al., 2020; Maoz et al., 2018; Park et al., 2019; Vatine et al., 2019). These
89 microfluidic models have certainly overcome several of the limitations of traditional culture
90 models. However, so far, they have not included microglial cells, an essential component
91 of the neurovascular unit (NVU), critically involved in the regulation of neuroinflammatory
92 activity (McConnell et al., 2017; Muoio et al., 2014; Streit and Kincaid-Colton, 1995).

93 In pathological states, microglia and astrocytes undergo complex changes increasing
94 their capacity to produce proinflammatory cytokines such as tumour necrosis factor-alpha
95 (TNF- α) (Lau and Yu, 2001; Wang et al., 2015), interleukin-1 β (IL-1 β), interleukin-6 (IL-
96 6), and interferon-gamma (IFN- γ), that increase the BBB permeability (De Vries et al.,
97 1996; Yarlagadda et al., 2009). TNF- α was shown to increase BBB permeability, induce
98 the activation of glia *in vivo* (Cheng et al., 2018; Neniskyte et al., 2014a), and potentiate
99 glutamate-mediated cytotoxicity, a process linked to neuronal death (Olmos and Lladó,
100 2014). Elevated levels of TNF- α have been found in traumatic brain injury (Frugier et al.,
101 2010), ischemic stroke (Zaremba and Losy, 2001), Alzheimer's (AD) (Jiang et al., 2011),
102 Parkinson's (PD) (Kouchaki et al., 2018), Multiple Sclerosis (MS) (Rossi et al., 2014), and
103 amyotrophic lateral sclerosis (ALS) (Cereda et al., 2008).

104 Here we describe how we leveraged the Human Emulation System[®] to build a
105 comprehensive Brain-Chip model to characterize cellular interactions underlying the
106 development of neuroinflammation. We have populated our Brain-Chip with human
107 primary astrocytes, pericytes, and iPSC-derived brain microvascular endothelial cells,
108 together with human iPSC-derived cortical neurons and microglial cell line. This Brain-
109 Chip supported a tissue relevant, multicellular architecture and the development of a tight
110 blood brain barrier, sustained over seven days in culture. Using next-generation
111 sequencing data and information retrieved from well-curated databases of signature gene
112 sets for the human cortex, we demonstrate that the Brain-Chip's transcriptomic signature
113 is closer to the adult cortical tissue than the conventional cell culture systems used to
114 study the BBB *in vitro* (Stone et al., 2019; Thomsen et al., 2015).

115 To simulate changes occurring during the early phases of neuroinflammation, we
116 perfused either the brain or the vascular side of the Brain-Chip with TNF- α . We
117 successfully reproduced key clinical features of neuroinflammation, such as disruption of
118 the BBB, astrocyte, and microglial activation, increased proinflammatory cytokine
119 release, capturing contributions of the individual brain cell types to inflammatory stimuli.
120 In summary, we present an *in vivo* relevant human Brain-Chip as a multicellular model
121 designed to investigate neurodegenerative pathogenesis and future applications,
122 including clinical studies that could lead to effective precision medicine treatments.

123

124 **RESULTS**

125 **Microengineered Human Brain-Chip Platform of the Neurovascular Unit**

126 We leveraged organ-on-chip technology and the recent progress in developing human
127 brain primary and iPSC-derived differentiated cells to generate a human Brain-Chip
128 model that enables the stimulation and monitoring of inflammatory responses. As
129 described previously, the Brain-Chip has two microfluidic channels, separated by a thin,
130 porous polydimethylsiloxane (PDMS) membrane that enables cellular communication
131 and supports coating with tissue-specific extracellular matrix (ECM) (Pediaditakis et al.,
132 2021). The top channel, we refer to as the "brain" channel of the chip, accommodates the
133 co-culture of key elements of the neurovascular unit (NVU), including excitatory and
134 inhibitory cortical neurons, microglia, astrocytes, and pericytes (McConnell et al., 2017).
135 The bottom channel, which we refer to as the "vascular" channel of the chip, is seeded
136 with human iPSC-derived brain microvascular endothelial-like cells (iBMECs) that create
137 a lumen-like structure (Wong et al., 2013), modelling the interface between the circulation
138 and the brain parenchyma (**Figure 1A**). We used cell proportions comparable to those

139 reported (von Bartheld et al., 2016; Shepro and Morel, 1993; Sultan and Shi, 2018; Xu et
140 al., 2010), with the understanding of the challenge in recapitulating the *in vivo* cellular
141 milieu.

142 To characterize the multicellular structure in the brain channel of the chip, we used
143 specific markers for each brain cell type, including microtubule-associated protein 2
144 (MAP2) for neurons, glial fibrillary acidic protein (GFAP), s100 β , and glutamate
145 transporter (GLAST) for astrocytes, ionized calcium-binding adaptor protein-1 (IBA-1) for
146 CD11b⁺ CD45^{low} microglia, neuron-gial antigen 2 (NG2), and smooth muscle alpha-actin
147 (α SMA) for pericytes (**Figures 1B, 1C and 1D**). Positive staining for the vesicular
148 glutamate transporter (VGLUT1) and the vesicular GABA transporter (VGAT) (**Figure**
149 **1E**), indicate the co-existence of excitatory and inhibitory neurons, respectively. To get
150 an initial evaluation of the functionality of the neurons in the Brain-Chip, we performed
151 immunofluorescent staining with synaptophysin (SYP), a nerve terminal marker synaptic
152 vesicle that stains mature presynaptic neurons. Our results show that MAP2 positive cells
153 expressed the synaptic marker synaptophysin (**Figure 1F**). The efficiency of synaptic
154 transmission is governed by the probability of neurotransmitter release, the amount of
155 neurotransmitter released from the presynaptic terminal. Additionally, our data
156 demonstrate the functional maturation of the human iPSC-derived neurons in the Brain-
157 Chip compared to transwells, as depicted by the secreted glutamate levels (**Figure 1G**),
158 suggesting functional differences between the two systems. To the best of our knowledge,
159 this is the first report on a human microphysiological system where inhibitory and
160 excitatory cortical neurons and primary microglia complement the cellular components of
161 BBB to form the neurovascular unit.

162 The establishment of the endothelial monolayer was assessed via staining for the tight
163 junction-specific marker, zona occludens-1 (ZO-1), Occludin, as well as the endothelial-
164 specific junctions PECAM1, which demonstrated that the endothelial-like cells form a
165 consistent morphology along the entire vascular channel of the chip (**Figure 2A**).
166 Additionally, we screened the endothelial-like cells we employed in our model for
167 expression of the epithelium markers Cadherin1 (CADH1), TRPV6, and Claudin-4. As
168 shown, we confirmed lack of expression in the endothelial-like cells, in contrast to the
169 human epithelial cell lines used as positive controls (**Figure S1A**). Once the endothelial-
170 like cells are cultured juxtaposed to pericytes, astrocytes, microglia, and neurons in the
171 Brain-Chip, they establish a tight barrier for seven days (**Figure 2B**). To this end, we
172 evaluated the apparent permeability (Papp) in Brain-Chips seeded with human iPSC-
173 derived brain microvascular endothelial-like cells from two different healthy donors
174 (Donor 1; RUCDR, Donor 2; iXcell) (**Figure 2B**). The obtained Papp values in our model
175 to 3 kDa, 10 kDa, 40 kDa, and 70 kDa dextran reached values as low as those reported
176 from *in vivo* studies (Shi et al., 2014; Yuan et al., 2009) (**Figure 2C**), routinely cited as
177 golden standards of apparent permeability. Moreover, the permeability values obtained
178 in the Brain-Chip were comparable within a specified range to those reported by previous
179 BBB studies with organ chips (Ahn et al., 2020; Vatine et al., 2019).

180 Findings on microglial location in the perivascular space highlight their interaction with
181 endothelial cells and support their influence on BBB integrity although, very few studies
182 have been conducted to delineate a direct link between microglia and barrier function
183 (Haruwaka et al., 2019a). On the other hand, astrocytes by providing a connection
184 between the endothelial blood flux and neurons (**Figure 2D**), are critical for the formation

185 and maintenance of the BBB (Alvarez et al., 2013). To explore the potential impact of
186 microglia and astrocytes on the barrier integrity, we measured the permeability to
187 cascade-blue 3-kDa dextran. Significant decrease in paracellular permeability in the
188 presence of microglia highlights its importance in the maintenance of the barrier integrity
189 in the Brain-Chip (**Figure S1B**). Further, we found significant increase in the permeability
190 in the absence of astrocytes, in line with their reported significant role in the stability and
191 maintenance of the BBB (Abbott et al., 2006). No significant effect in the permeability was
192 detected by eliminating neurons, the most abundant cell in the Brain-Chip. Taken
193 together, all the above support the hypothesis that the decrease in permeability in the
194 Brain-Chip following challenge with TNF- α is specifically driven from the microglia and
195 the astrocytes, rather than from a technical/mechanical obstacle, such as clogging of the
196 pores.

197 Furthermore, the comparison to chips that contain only iPSC-derived brain microvascular
198 endothelial-like cells provides further reassurance on the contribution of the supporting
199 cells in the Brain-Chip that also contains pericytes, astrocytes, microglia, and neurons
200 (Keaney and Campbell, 2015; Obermeier et al., 2013) (**Figure S1C**) in the stability of the
201 barrier. We also confirmed that the cells in the vascular channel expressed the brain
202 endothelium-specific glucose transporter, GLUT-1 (Veys et al., 2020) (**Figure S1D**), and
203 showed internalization of transferrin (**Figure S1E**), an essential mechanism for transport
204 across the BBB leveraged for delivery of therapeutic antibodies (Jones and Shusta,
205 2007). Further characterization of iBMECs via FACS analysis confirmed the expression
206 of the brain endothelium-specific glucose transporter, GLUT-1, transferrin receptor, and
207 efflux transporters in the BBB, such as P-glycoprotein (P-gp) and MRP-1 (**Figure S1F**),
208 of additional reassurance on the potential of the model in evaluating the ability of
209 developing therapeutics to enter the brain.

210

211 **Transcriptomic Comparison of the Human Brain-Chip Versus Conventional** 212 **Transwell Systems and Adult Human Tissue**

213 After confirming the *in vivo* relevant cell composition and barrier function, we assessed
214 the extent of similarities in gene expression between the Brain-Chip and the adult human
215 cortex tissue, as well as the differences compared to the transwell brain model, the most
216 commonly used cell culture system for modeling brain *in vitro*. Using the same cell
217 composition and experimental conditions in transwells and Brain-Chip cultures, we
218 performed RNAseq analyses on days 5 and 7 of culture. Expression of specific markers
219 for each of the cell types seeded, confirmed their representation in the culture at the time
220 of the analyses. Principal Component Analysis (PCA) showed clear separation between
221 the samples of the two models in the 2-dimensional space determined by the first two
222 PCs explaining 47.5% of the total variance in the data (**Figure 3A**). Unlike transwells,
223 Brain-Chips were clustered together in the 2D PCA space, which indicates their
224 transcriptomic “stability” across the days in culture (**Figure 3A**). Next, we examined the
225 differential gene expression (DGE) in Brain-Chips compared to transwells. Out of the
226 57,500 genes annotated in the genome, 5695 were significantly differentially expressed
227 (DE) between these samples: 3256 and 2439 genes were up- and down-regulated,
228 respectively (**Figure 3B**). Next, using the information of the up- and down- DE genes, we
229 performed gene ontology (GO) enrichment analysis to identify the significantly enriched
230 biological processes in the two systems (Ashburner et al., 2000; Mi et al., 2013). In Brain-

231 Chips we identified significantly enriched pathways (FDR p -value ≤ 0.05) of the Brain
232 channel related to the extracellular matrix organization, cell adhesion, and tissue
233 development (**Figure 3C**). Evidence has been accumulated that activity-dependent
234 aggregation and proteolysis of ECM (extracellular matrix organization) and associated
235 molecules shape synaptogenesis, synapse maturation, and synaptic circuit remodeling
236 (Ferrer-Ferrer and Dityatev, 2018). Extracellular matrix accelerates the formation of
237 neural networks and communities in a neuron-glia co-culture (Lam et al., 2019). In
238 contrast, axonogenesis, axon guidance, chemotaxis, neurogenesis, neuron migration, and
239 cell differentiation pathways were significantly enriched in transwells (**Figure 3D**),
240 supporting the hypothesis of incomplete neuronal maturation in these systems (Hesari et
241 al., 2016; Sances et al., 2018). A basic property of immature neurons is their ability to
242 change position from the place of their final mitotic division in proliferative centers of the
243 developing brain to the specific positions they will occupy in a given structure of the adult
244 nervous system (Rakic, 1990). Proper acquisition of neuron position, attained through the
245 process of active migration and chemotaxis (Cooper, 2013).
246 Lastly, we used the Transcriptomic Signature Distance (TSD) (Manatakis et al., 2020) to
247 calculate the Brain-Chip's and transwell's transcriptomic distances from the adult human
248 cortex tissue. We were able to show that the Brain-Chip exhibits higher transcriptomic
249 similarity (smaller transcriptomic distance) to the adult human cortex on either day of
250 culture compared to the transwells (**Figure 3E**), by leveraging next-generation
251 sequencing data and information retrieved from the Human Protein Atlas database
252 providing signature gene sets characteristic for the human brain (Uhlén et al., 2015). To
253 further support our conclusions, we used the cerebral cortex RNA-seq data, from two
254 different human donors (donor 9861 and 10021), available in the Allen Brain Atlas
255 (Available from: human.brain-map.org). For each donor, we measured the transcriptomic
256 signature distances (TSDs) between the corresponding cerebral cortex samples and (i)
257 Brain-Chip and (ii) Transwells on Days 5 and 7. For both donors, the results clearly
258 indicate that for both days, our Brain-Chips are statistically significantly closer to human
259 cerebral cortex as compared to transwells (**Figure S2**). Cumulatively, these findings
260 demonstrate that the Brain-Chip recapitulates the cortical brain tissue more closely than
261 conventional cell culture systems such as transwells.

262 263 **TNF- α -Induced Neuroinflammation in the Brain-Chip**

264 Neuroinflammation is emerging as a key mechanism in the progress of several infectious
265 and neurodegenerative diseases (Guzman-Martinez et al., 2019b; Perry et al., 2007a).
266 While the pathways driving neuroinflammation in response to infection have been
267 delineated, the exact mechanisms that trigger and sustain the activation of glia (microglia
268 and astrocytes) and the direct association with the barrier function remain unclear.
269 To model neuroinflammation in the Brain-Chip, we perfused TNF- α directly in the brain
270 channel at a concentration of 100 ng/mL starting on day five of culture (**Figures 4A and**
271 **S3A**) for two days. The concentration of 100 ng/mL TNF- α was chosen based on previous
272 studies, where this concentration stimulated proinflammatory factors to be released and
273 compromised the barrier integrity (Rochfort et al., 2014, 2016). As the majority of
274 neuroinflammatory responses are elicited by the supportive glial cells, in particular
275 microglia and astrocytes, the incorporation and evaluation of these cell types in *in vitro*
276 assay systems is of particular interest in the pharmaceutical field.

277 To confirm the advantage of the Brain-Chips containing both microglia and astrocytes,
278 the key cellular mediators of neuroinflammatory processes, we compared TNF- α -induced
279 secretion of inflammatory cytokines in Brain-Chip in the presence or absence of microglia
280 or astrocytes in the brain channel. We found significantly increased levels of interleukin-
281 1 β (IL-1 β), interleukin-6 (IL-6), and interferon-gamma (IFN γ) in the effluent of the Brain-
282 Chips containing microglia and astrocytes, following 48 h of exposure to TNF- α (**Figures**
283 **4B to D**). Notably, absence of microglia resulted in compromised induction of both IL-1 β
284 and IFN γ , while it prevented any change in IL-6 secretion, in contrast to the high levels of
285 IL-6 detected in the microglia-containing Brain-Chip (**Figures 4B to D**). These findings
286 capture the microglia-dependent inflammatory responses to TNF- α in the Brain-Chip, in
287 line with previous studies.

288 These findings demonstrate that Brain-Chips containing microglia respond to noxious
289 stimuli such as TNF- α by mounting an inflammatory response in a manner similar to that
290 shown in *in vivo* studies (Block et al., 2007; Brás et al., 2020; Haruwaka et al., 2019b;
291 Kuno et al., 2005; Merlini et al., 2021; Perry et al., 2007b).

292 Although microglia cells are the primary source of cytokines, astrocytes do also
293 perpetuate the destructive environment via secretion of various chemokines and
294 proinflammatory cytokines, including IL-1 β and IFN γ (Rothhammer and Quintana, 2015),
295 in line with our findings. Interestingly, TNF- α induced IL-6 secretion directly from the
296 microglia but not from the astrocytes, that required the presence of microglia for induction
297 of cytokines secretion. Cumulatively, our data suggest the operation of different
298 regulatory mechanisms and cell-to-cell interactions driving the cytokine responses of glial
299 cells during inflammation. These findings indicate the potential of the Brain-Chip to
300 critically support the development of specific new therapeutic approaches for patients.

301 In line with the increased cytokine release, TNF- α exposure led to activation of microglia
302 and astrocytes, as depicted by significant increases in CD68 positive cells or the
303 proportion of GFAP-positive cells respectively (**Figures 4E to 4H and S3B, S3C**),
304 recapitulating *in vivo* findings for glial cells that constitute the first response to
305 inflammatory and infectious stimuli (Boche et al., 2019; Sun et al., 2008). Astrocytes
306 exposed to TNF- α displayed a significant change in their morphology, transitioning from
307 a polygonal shape towards a more elongated (stellate) shape (**Figure 4I**). Further, we
308 detected pericyte activation, in line with the notion of the importance of NG-2 reactive
309 pericytes in neuroinflammation (Ferrara et al., 2016) (**Figure 4J and 4K**), although we
310 did not detect any significant effect on the total nuclei count (**Figure S3D**). Our studies
311 revealed no differences in the abundance of Ki67-positive cells between the control and
312 treated groups, suggestive of TNF- α -induced activation of the existing, astrocytes, rather
313 than generation of new astrocytes (**Figures 3SE and 3SF**).

314 In addition, exposure to TNF- α resulted in the loss of neuronal immunoreactivity of the
315 cytoskeletal microtubule-associated protein (MAP-2) compared to the control, in neurons,
316 suggesting that TNF- α induced neuronal injury/damage (**Figures 4F and 4L**), in line with
317 the described neurotoxic effects of inflammatory mediators (Neniskyte et al., 2014b).
318 Excessive brain TNF- α levels have been associated with the compromised activity of the
319 glutamate transporters, which results in an increase in glutamate levels. The secreted
320 glutamate levels in the effluent of the brain channel of the chip in control Brain-Chips
321 remained stable on days 5, 6 and 7 of culture (**Figure 1G**), while they increased
322 significantly increased following two days of exposure to TNF- α (**Figure 4M**). These data

323 corroborate reports from *in vitro* and *in vivo* studies linking glutamate-induced
324 excitotoxicity to neuroinflammation (Olmos and Lladó, 2014; Rossi et al., 2014; Ye et al.,
325 2013).

326 Strong experimental evidence has demonstrated the multifaceted effects of TNF- α on the
327 BBB anatomy and function, via its direct action on the endothelium as well as the
328 downstream effects via induction of associated proinflammatory factors (Trickler et al.,
329 2005; Zhao et al., 2007). We found that in the Brain-Chip, the perfusion of the brain
330 channel with TNF- α (100 ng/mL) for two days, ensued loss of the integrity of the tight
331 junctions, as demonstrated by diffuse ZO-1 staining (**Figures 5A**). Furthermore, the
332 expression of intercellular adhesion molecule 1 (ICAM-1), a hallmark of inflammation-
333 promoting adhesion and transmigration of circulating leukocytes across the BBB
334 (Marchetti and Engelhardt, 2020), was also significantly induced (**Figure 5A**).
335 Assessment of the barrier function revealed a significant increase in permeability to 3kDa
336 dextran in the TNF- α treated Brain-Chip, in a time dependent-manner (**Figure 5B**).
337 Furthermore, we show that the changes in barrier permeability were only evident in the
338 presence of microglia (**Figure 5C**), confirming previous findings on the critical role of this
339 cell in driving BBB dysfunction (Nishioku et al., 2010). To further support this hypothesis,
340 we used Minocycline to inhibit the induction of reactive microglia (Ai et al., 2005; Henry
341 et al., 2008). Reportedly, Minocycline reduces the characteristic BBB leakage in rodent
342 models of brain diseases, such as hypoxia, ischemia, and Alzheimer's disease (Ryu and
343 McLarnon, 2006; Yang et al., 2015; Yenari et al., 2006). Our findings add on our
344 understanding on barrier function in the human Brain-Chip as a result of TNF- α induced
345 inflammation, as they also include the response of microglia (**Figure 5D**).

346 These results taken together show how the Brain-Chip can be applied to characterize
347 specific changes in cell-cell interactions underlying the development and progress of
348 neuroinflammation.

349

350 **Neuroinflammation in the Brain-Chip Induced by Vascular Exposure to TNF- α**

351 Although pathology locally in the brain is associated with massive production of
352 proinflammatory cytokines (neuroinflammation), reports show that systemic
353 infections/inflammatory states spreading to the brain through the vascular system, can
354 also induce inflammation in the brain and alter the progression of chronic
355 neurodegenerative diseases (Perry, 2004). To assess how systemic (through the
356 vascular channel) administration of TNF- α affects the cells in the brain channel (**Figure**
357 **6A and S4A**), we first performed immunostaining for CD68, GFAP, and NG2 two days
358 after vascular administration of TNF- α , that revealed activation of microglia, astrocytes,
359 and respectively (**Figure 6B to 6F**), while we did not detect any significant effect on the
360 total nuclei count (**Figure 6G**).

361 Next, we characterized markers indicative of neuroinflammation. We found significantly
362 higher levels of IFN γ , IL-1 β , and IL-6 in the effluent collected from the brain channel,
363 following two days of vascular exposure to TNF- α , compared to the untreated group
364 (**Figure 6H to 6J**). These findings are consistent with published studies showing that
365 TNF- α crossing through the BBB activates the microglia and induced the release of
366 proinflammatory cytokines, resulting in further propagation of the inflammatory process in
367 the brain (Qin et al., 2007; Tangpong et al., 2006). We also found higher levels of IFN γ ,
368 IL-1 β , and IL-6 in the vascular channel media in the TNF-treated model group compared

369 to the untreated group, all of which contribute to increase the barrier permeability (**Figure**
370 **S4B**). However, no neuronal damage was detectable, as per the number of MAP2-
371 positive neurons and the secreted glutamate levels (**Figures 6K and 6L**). Thus, vascular-
372 mediated challenge of the brain with TNF- α induces neuroinflammation, although
373 relatively milder compared to that following direct exposure to TNF- α , administered
374 through the brain channel.

375 Immunofluorescence analysis showed significantly attenuated expression of the tight
376 junction protein ZO-1 and increased expression of ICAM-1 in the TNF- α treated chips
377 compared to the control chips (**Figures 6M**). Further, the barrier permeability to 3kDa
378 dextran was significantly increased in the TNF- α treated chips (**Figure 6N**). Overall, these
379 findings were similar to those described in detail above, in the neuroinflammation model
380 above (**Figure 5A, 5B and 5C**).

381 Brain barriers are uniquely positioned to communicate signals between the central
382 nervous system and peripheral organs. The BBB cells (endothelial cells, pericytes and
383 astrocytes) respond to signals originating from either side by changes in permeability,
384 transport, and secretory functions (Cunningham et al., 2009; Erickson and Banks, 2018;
385 Verma et al., 2006). It has been previously shown that TNF- α crosses the intact BBB by
386 a receptor-mediated transport system, upregulated by CNS trauma and inflammation
387 (Gutierrez et al., 1993; Pan and Kastin, 2002; Pan et al., 2003a). Free traffic of
388 radioactively labelled TNF- α from blood to brain and cerebrospinal fluid (CSF) has been
389 shown in mice (Gutierrez et al., 1993; Pan et al., 1997), as well as in monolayers of
390 cultured cerebral microvessel endothelial cells (Pan et al., 2003b). We measured the
391 levels of TNF- α in effluent from both the brain and vascular channels (**Figure S4C**) and
392 identified significantly lower basal levels in the former (control condition). Our results
393 confirm that TNF- α can cross through the intact barrier in either direction, i.e., brain or
394 vascular. Also, barrier disruption resulted in significantly increased TNF- α levels from the
395 vascular compartment into the brain compartment and vice versa (**Figure 7A and 7B**).

396 Still, a knowledge gap remains in our in-depth understanding of the interplay between
397 gain/loss of function of drug transporters and their role in the development of neurological
398 diseases, whether changes in transporter expression are a cause or consequence of
399 these diseases. Glucose transporter-1, GLUT-1 is the major cerebral glucose transporter,
400 and is expressed at particularly high levels in endothelial cells that line the brain capillaries
401 (Vannucci, 1994). Although decreases in GLUT-1 expression is a well-accepted
402 biomarker for degenerative and inflammatory brain diseases (Winkler et al, 2015), how it
403 is associated to their pathogenesis remains elusive. To this purpose, we measured the
404 GLUT-1 expression in both TNF- α treatment conditions (brain or vascular side dosing)
405 compared to the control group. Analysis of immunofluorescence images showed
406 substantial decrease in GLUT-1 expression upon TNF- α treatment as compared to the
407 control group (**Figure 7C and 7D**), showing the sensitivity of the Brain-Chip to capture
408 the direct effect of TNF- α on GLUT-1 transporter. Although there are differences
409 associated with the specific route of administration of TNF- α in the inflammation-induced
410 mechanisms, exposure through the brain or the vascular channel represent relevant *in*
411 *vivo* conditions. All the above taken together, suggest that the Brain-Chip may advance
412 our understanding on the molecular mechanisms underlying function of BBB transporters
413 in basal and disease states.

414

415 DISCUSSION

416 In the present study, we designed a microfluidic model, a human Brain-Chip, that
417 recreates several functional features of the neurovascular unit. Cortical neurons,
418 astrocytes, microglia, and pericytes compose the parenchymal basement membrane
419 (brain side) whereas astrocytic end-feet embracing the abluminal aspect of the brain
420 microvessels (vascular side). Astrocytes and microglia were maintained in a resting state
421 in coordination with low levels of cytokine secretion. The endothelial-like monolayer within
422 the human Brain-Chip sustained the expression of tight junction proteins and showed low
423 barrier permeability levels for seven days in culture, similar to those reported for the
424 human brain *in vivo* (Shi et al., 2014; Yuan et al., 2009), for seven days in culture.

425 By leveraging next-generation sequencing data and information retrieved from well-
426 curated databases providing signature gene sets characteristic for the human cortex, we
427 were able to show that the Brain-Chip exhibits higher transcriptomic similarity to the adult
428 cortical tissue than the transwells, both models with the same cellular composition. These
429 data complement previous reports on the advantages of the microfluidic organ-chip
430 systems to provide a better tissue-relevant microenvironment compared to other
431 commonly used conventional culture systems (Pediaditakis et al., 2021; Sances et al.,
432 2018). Most importantly, our findings demonstrate the closeness of the Brain-Chip to the
433 adult human cortex tissue and the cells' maturation state after seven days in culture.

434 Neuroinflammation emerges as an essential process in the pathogenesis of
435 neurodegenerative diseases. Several studies have shown direct effects of the activated
436 microglia, astrocytes, and pericytes and the secreted cytokines in the brain and BBB
437 functions (Biswas et al., 2020; Freitas-Andrade et al., 2020; Horng et al., 2017; Liebner
438 et al., 2018; Sofroniew, 2015; Sweeney et al., 2019). TNF- α , a key mediator of
439 inflammation, impairs neuronal function, suppresses long-term hippocampal potentiation
440 (LTP), a mechanism essential for memory storage and consolidation (Cunningham et al.,
441 1996), and affects synaptic transmission (Singh et al., 2019). Further, TNF- α levels have
442 been found markedly elevated in the brains of patients with Alzheimer's disease (Heneka
443 and O'Banion, 2007), indicative of the active inflammatory process in the disease. It has
444 been proposed that systemic inflammation exacerbates neuroinflammation and
445 neurodegeneration via circulating pro-inflammatory factors (Perry et al., 2007a), such as
446 TNF- α , crossing the BBB via active transport (Osburg et al., 2002; Pan and Kastin, 2007)
447 or through the compromised barrier (Franzén et al., 2003; Trickler et al., 2005). Despite
448 the increasing experimental and clinical evidence on the connection between
449 neuroinflammation, neurodegeneration, and, ultimately, neuronal death, the development
450 of effective therapeutic targets is still slow. A major factor contributing to the latter is that
451 there is still lack of specific models for the onset and progress of human brain diseases.
452 Most of the existing *in vitro* BBB models do not incorporate neurons and glia in the blood-
453 brain barrier cell systems, resulting in incomplete modeling of the inflammatory
454 responses.

455 In the present study, we characterized the Brain-Chip responses upon exposure to TNF-
456 α via two distinct routes, either directly through the brain channel or via the vascular
457 channel, where TNF- α reaches the brain cells by crossing through the barrier either
458 actively or paracellularly. We show that the brain's exposure to TNF- α , either directly or
459 through the BBB, results in activation of microglia and astrocytes, secretion of cytokines,
460 and neuronal damage. As expected, exposure to TNF- α induced significant changes in

461 tight junction formation that compromised the barrier permeability and induced adhesion
462 molecules such as ICAM-1, which propagated the inflammatory response by facilitating
463 the recruitment of the immune cells to the brain (Marchetti and Engelhardt, 2020). We
464 expect that future studies set to characterize the precise sequence of events following
465 exposure to systemic- or tissue-induced inflammatory injury might provide important,
466 targetable hints for critical cell-driven mechanisms in neuroinflammation.
467 The comprehensive Brain-Chip model presented here can enhance our current capability
468 to interrogate both brain barrier dysfunction and neuron-glia interactions underlying the
469 onset and progress of neuroinflammation, for the benefit of human patients.

470 471 **METHODS**

472 **Brain-Chip Microfabrication and Zoë[®] Culture Module.** The design and fabrication of
473 Organ-Chips used to develop the Brain-Chip was based on previously described
474 protocols (Huh et al., 2013). The chip is made of transparent, flexible
475 polydimethylsiloxane (PDMS), an elastomeric polymer. The chip contains two parallel
476 microchannels (a 1 × 1 mm brain channel and a 1 × 0.2 mm vascular channel) that are
477 separated by a thin (50 μm), porous membrane (7 μm diameter pores with 40 μm spacing)
478 coated with E.C.M. (400 μg/mL collagen IV, 100 μg/mL fibronectin, and 20 μg/mL laminin,
479 at the brain and vascular side). Brain-Chips were seeded with human iPSC-derived
480 glutamatergic and GABAergic neurons (NeuCyte;1010) at a density of 4x10⁶ cells/mL and
481 2x10⁶ cells/mL respectively, co-cultured with, human primary astrocytes (NeuCyte;1010)
482 at a density of 2x10⁶ cells/mL, human microglial cell line (ATCC; CRL3304) at a density
483 of 2x10⁵ cells/mL, and primary pericytes (Sciencell;1200) at a density of 1.5x10⁵ cells/mL,
484 using "seeding medium" (NeuCyte), and incubated overnight. The next day, human iPSC-
485 derived Brain Microvascular Endothelial-like cells were seeded in the vascular channel at
486 a density of 14 to 16x10⁶ cells/mL using human serum-free endothelial cell medium
487 supplemented with 5% human serum from platelet-poor human plasma (Sigma) and
488 allowed to attach to the membrane overnight. Chips were then connected to the Zoë[®]
489 Culture Module (Emulate Inc.). At this time, the medium supplying the brain channel was
490 switched to maintenance medium (Neucyte), and the serum of the vascular medium was
491 lowered to 2%. Chips were maintained under constant perfusion at 60 μL/h through both
492 chips' brain and vascular channels until day seven.

493
494 **Brain Transwell Model.** The conventional cell cultures (transwells) and the Brain-Chips
495 were seeded using the same ECM composition as well as cell composition, media
496 formulations and seeding density. At the first experimental day (D0) the cortical
497 (Glutamatergic and GABAergic subtypes) neurons, astrocytes, microglia, and pericytes
498 were seeded on the apical side, followed by the seeding of the endothelial cells (D1) on
499 the basolateral side of the 0.47 cm² Transwell-Clear permeable inserts (0.4-μm pore
500 size). For the apical compartment we used NeuCyte medium, while for the basolateral
501 compartment we used hESFM with 5% human serum from platelet-poor human plasma.
502 The cells maintained under static conditions throughout the duration of the experiment
503 (D8). The culture medium was replaced daily in both compartments.

504
505 **Differentiation of iPSCs into Brain Microvascular Endothelial-like Cells.** Human
506 iPSCs (Donor 1: RUCDR; ND50028, Donor 2: iXcell; 30HU-002) were passaged onto

507 Matrigel in mTeSR1 medium for 2 to 3 days of expansion. Colonies were singularized
508 using Accutase (STEMCELL; 07920) and replated onto Matrigel-coated plates at a
509 density $25\text{-}50 \times 10^3$ cells/cm² in mTeSR1 supplemented with 10 mM Rho-associated
510 protein kinase (ROCK) inhibitor Y-27632 (STEMCELL; 72304). Singularized Human
511 iPSCs were expanded in mTeSR1 for 3 days. Cells were then treated with 6 mM
512 CHIR99021 (STEMCELL; 72052) in DeSR1: DMEM/Ham's F12 (Thermo Fisher
513 Scientific; 11039021), 1X MEM-NEAA (Thermo Fisher Scientific; 10370021), 0.5%
514 GlutaMAX (Thermo Fisher Scientific; 35050061), and 0.1 mM b-mercaptoethanol
515 (Sigma). On Day 1, the medium was changed to DeSR2: DeSR1 plus 1X B27 (Thermo
516 Fisher Scientific) daily for another 5 days. On day 6, the medium was switched to
517 hECSR1: hESFM (ThermoFisher Scientific) supplemented with bFGF (20 ng/mL), 10 mM
518 Retinoic Acid, and 1X B27. On day 8, the medium was changed to hECSR2 (hECSR1
519 without R.A. or bFGF). On day 10 cells were dissociated with TrypLE™ and plated at
520 1×10^6 cells/cm² in hESFM supplemented with 5% human serum from platelet-poor
521 human plasma onto a mixture of collagen IV (400 µg/mL), fibronectin (100 µg/mL), and
522 laminin (20 µg/mL) coated flasks at a density of 1×10^6 cells/cm². After 20 min the flasks
523 were rinsed using hESFM with 5% human serum from platelet-poor human plasma with
524 Y-27632 as a selection step to remove any undifferentiated cells and allowed to attach
525 overnight (Qian et al., 2017).

526

527 **Morphological Analysis.** Immunocytochemistry was conducted as previously described
528 (Pediaditakis et al., 2021). Cells were blocked on the Brain-Chip in phosphate-buffered
529 saline (PBS) containing 10% donkey serum (Sigma) at 4°C overnight. Saponin 1% was
530 used to permeabilize membrane when required. Primary antibodies were MAP2 (Thermo
531 Fisher Scientific; MA512826), VGLUT1 (Thermo Fisher Scientific; 48-2400),
532 Synaptophysin (Abcam; 32127), GFAP (Abcam; ab53554), GLAST (Invitrogen; PA5-
533 19709), s100β (Abcam; 52642), NG2 (Abcam; ab83178), αSMA (Abcam; 7817), IBA1
534 (FUJIFILM; 019-19741), CD68 (Abcam; ab213363), ICAM-1 (R&D Systems; BBA3), Ki67
535 (Abcam; 197234), ZO-1 (Thermo Fisher Scientific; 402200), Occludin (Invitrogen; OC-
536 3F10), Claudin-4 (Invitrogen; 329494), TRPV6 (Proteintech; 13411-1-AP), PECAM1
537 (Thermo Fisher Scientific; RB-1033-P1), CD11b (Invitrogen; MA1-80091), CD45
538 (Invitrogen; 17-0409-42), GLUT1 (Thermo Fisher Scientific; SPM498), P-gp (Thermo
539 Fisher Scientific; p170(F4)), MRP-1 (Millipore; MAB4100), Transferrin receptor (Abcam;
540 216665). Chips treated with corresponding Alexa Fluor secondary antibodies (Abcam)
541 were incubated in the dark for 2 h at room temperature. Cells were then counterstained
542 with nuclear dye DAPI. Images were acquired with an inverted laser-scanning confocal
543 microscope (Zeiss LSM 880).

544

545 **Flow Cytometry.** Cells were dissociated with Accutase, fixed in 1% PFA for 15 min at
546 room temperature, and then washed with 0.5% bovine serum albumin (BSA) (Bio-Rad)
547 plus 0.1% Triton X-100 three times. Cells were stained with primary and secondary
548 antibodies diluted in 0.5% BSA plus 0.1% Triton X-100. Data were collected on
549 a FACSCelesta flow cytometer (Becton Dickinson) and analyzed using FlowJo.
550 Corresponding isotype antibodies were used as FACS (fluorescence-activated cell
551 sorting) gating control. Details about antibody source and usage are provided in table.

552

553 **Visualization of Transferrin Receptor Internalization.** Human iPSC-derived Brain
554 Microvascular Endothelial-like cells were treated with 25 µg/mL fluorescent transferrin
555 conjugate (Thermo Fisher Scientific) and incubated at 37°C for 30 min. Cells were
556 washed twice with LCIS and fixed with P.F.A. Cells labeled with Alexa Fluor™ Plus 647
557 Phalloidin and DAPI and then imaged with Zeiss LSM 880.

558
559 **Scanning Electron Microscopy.** At the indicated timepoints Brain-Chips were fixed at
560 room temperature, for 2 hours in 2.5% Glutaraldehyde solution and washed three times
561 with 0.1M sodium cacodylate (NaC) buffer. Concomitantly, the chip was trimmed using a
562 razor so that the lateral and top chunks of PDMS are removed and the top channel is
563 revealed. Afterwards, the samples were fixed with 1% osmium tetroxide (OsO₄) in 0.1M
564 NaC buffer for 1 hour at room temperature and dehydrated in graded ethanol. The chip
565 samples were dried using the chemical drying agent Hexamethyldisilazane (HMDS),
566 sputter coated with platinum and images were acquired using the Hitachi S-4700 Field
567 Emission Scanning Electron Microscope.

568
569 **Permeability Assays.** To evaluate the establishment and integrity of the barrier, 3 kDa
570 Dextran, Cascade Blue, was added to the vascular compartment of the Brain-Chip at 0.1
571 mg/mL. After 24 h, effluent from both channels was sampled to determine the dye's
572 concentration that had diffused through the membrane. The apparent paracellular
573 permeability (P_{app}) was calculated based on a standard curve and using the following
574 formula:

575
576
$$P_{app} = \frac{Q_R * Q_D}{SA * (Q_R + Q_D)} * \ln \left[1 - \frac{C_{R,O} * (Q_R + Q_D)}{(Q_R * C_{R,O} + Q_D * C_{D,O})} \right]$$

577
578 where SA is the surface area of sections of the channels that overlap (0.17cm²), Q_R and
579 Q_D are the fluid flow rates in the dosing and receiving channels respectively, in units of
580 cm³/s, $C_{R,O}$ and $C_{D,O}$ are the recovered concentrations in the dosing and receiving
581 channels respectively, in any consistent units.

582
583 **TNF-α Treatment.** To mimic the inflammatory condition, cells were treated on either brain
584 or vascular channel with TNF-α (Tumor Necrosis Factor-α, R&D Systems; 210-TA). The
585 treatment was initiated after the formation of a confluent monolayer at ~5 days in culture.
586 Cells were further incubated in a culturing medium, including TNF-α (100 ng/mL) up to 48
587 h.

588
589 **Western Blotting.** RIPA cell lysis buffer supplemented with protease and phosphatase
590 inhibitors (Sigma) was used for the extraction of total protein from either brain or vascular
591 channel. The Auto Western Testing Service was provided by RayBiotech, Inc. (Peachtree
592 Corners, GA USA). 0.2 mg/mL sample concentration was loaded into the automated
593 capillary electrophoresis machine. Glial fibrillary acidic protein (GFAP) and
594 Gluceraldehyde-3-phosphate dehydrogenase (GAPDH) antibody provided by
595 RayBiotech was used as the loading control.

596

597 **ELISA Analysis.** The levels of IFN γ , IL-1 β , and IL-6 were measured by M.S.D. 96-well
598 plate Human Pro-Inflammatory V-PLEX Human Pro-Inflammatory Assay kits. The
599 secreted levels of Glutamate were measured by Glutamate Assay Kit (Fluorometric)
600 (Abcam; ab138883).

601
602 **RNA Isolation and Sequencing.** According to manufacturer's guidelines, we used
603 TRIzol (TRI reagent, Sigma) to extract the RNA. The collected samples were submitted
604 to GENEWIZ South Plainfield, NJ, for next-generation sequencing. After quality control
605 and RNA-seq library preparation the samples were sequenced with Illumina HiSeq 2x150
606 system using sequencing depth ~50M paired-end reads/sample.

607
608 **RNA Sequencing Bioinformatics.** Using Trimmomatic v.0.36 we trimmed the sequence
609 reads and filtered-out all poor-quality nucleotides and possible adapter sequences. The
610 remained trimmed reads were mapped to the Homo sapiens reference genome GRCh38
611 using the STAR aligner v2.5.2b. Next, using the generated BAM files we calculated for
612 each sample the unique gene hit-counts by using the featureCounts from the Subread
613 package v.1.5.2. It is worth noting that only unique reads that fell within the exon region
614 were counted. Finally, the generated hit-counts were used to perform DGE analysis using
615 the "DESeq2" R package (Love et al., 2014). The thresholds used for all the DGE
616 analyses were: $|\log_2(\text{Fold Change})| \geq 1$ and adjusted p-value ≤ 0.01 .

617
618 **GO term Enrichment Analysis.** The DE genes identified after performing the DGE
619 analyses were subjected to Gene Ontology (GO) enrichment analysis. The GO terms
620 enrichment analysis was performed using the Gene Ontology knowledgebase (Gene
621 Ontology Resource <http://geneontology.org/>).

622
623 **GTEX Portal provides 255 RNA-seq Samples for Human Brain-Cortex.** From these
624 samples only 5 were from healthy individuals and had RNA Integrity Number larger than
625 8 ($\text{RIN} \geq 8$), which indicates good RNA-quality. To create a "balanced" dataset (i.e., 4
626 samples per condition) from these 5 samples, we selected the group of 4 that had the
627 smallest variance. We combined the selected samples with the 16 samples from our
628 healthy models (i.e., Brain-Chips and transwells on Days 5 and 7). Next, we used the
629 "remove Batch Effect" function of the "limma" R package (Ritchie et al., 2015) to remove
630 shifts in the means between our samples (Brain-Chips and transwells) and the 4 human
631 Brain-Cortex samples retrieved from GTEx portal (Lonsdale et al., 2013). The same
632 process was repeated to combine the 16 samples from our healthy models with
633 each one of the two different cerebral cortex RNA-seq data from two different human
634 donors (donor 9861 and 10021) available in the Allen Brain Atlas (© 2010 Allen Institute
635 for Brain Science. Allen Human Brain Atlas. Available from: human.brain-map.org). This
636 dataset used for the calculation of the Transcriptomic Signature Distances (TSDs)
637 (Manatakis et al., 2020).

638
639 **Transcriptomic Signature Distance (TSD) Computation.** TSD is a novel distance
640 metric based on information theory that allows us to reliably assess the transcriptomic
641 similarity between organ tissue samples. The TSD uses (i) next-generation sequencing
642 data and (ii) tissue-specific genes (i.e., signature genes) provided by the well-curated and

643 widely accepted Human Protein Atlas (HPA) project (Uhlén et al., 2015), and calculates
644 the transcriptomic distance of a tissue sample (e.g., Brain-Chip or transwell) from the
645 reference tissue (in our case the Human Brain-Cortex). As signature genes we used the
646 set of 2587 genes that are reported to have significantly elevated expression levels in the
647 brain tissue compared to other tissue types (Uhlén et al., 2015).

648

649 **Statistical Analysis.** All experiments were performed in triplicates. Analysis of
650 significance was performed by using two-way ANOVA with Tukey's multiple comparisons
651 test or unpaired t-test depending on the data sets. The error bars represent standard error
652 of the mean (s.e.m); p-values < 0.05 and above were considered significant.

653

654 **Data Availability**

655 All data generated or analyzed during this study are included in this published article.
656 RNA sequencing data have been deposited in the National Center for Biotechnology
657 Information Gene Expression Omnibus (GEO).

658

659 **Code Availability**

660 All the code for the analysis in this report is derived from previously published reports. It
661 is also explained and cited in the appropriate material and methods section.

662

663 **REFERENCES**

664 Abbott, N.J., Rönnbäck, L., and Hansson, E. (2006). Astrocyte-endothelial interactions at
665 the blood-brain barrier. *Nature Reviews Neuroscience* 7, 41–53.

666 Ahn, S.I., Sei, Y.J., Park, H.J., Kim, J., Ryu, Y., Choi, J.J., Sung, H.J., MacDonald, T.J.,
667 Levey, A.I., and Kim, Y.T. (2020). Microengineered human blood–brain barrier platform
668 for understanding nanoparticle transport mechanisms. *Nature Communications* 11.

669 Ai, L.W., Yu, A.C.H., Lok, T.L., Lee, C., Le, M.W., Zhu, X., and Tso, M.O.M. (2005).
670 Minocycline inhibits LPS-induced retinal microglia activation. *Neurochemistry*
671 *International* 47, 152–158.

672 Alvarez, J.I., Katayama, T., and Prat, A. (2013). Glial influence on the blood brain barrier.
673 *GLIA* 61, 1939–1958.

674 Ashburner, M., Ball, C.A., Blake, J.A., Botstein, D., Butler, H., Cherry, J.M., Davis, A.P.,
675 Dolinski, K., Dwight, S.S., Eppig, J.T., et al. (2000). Gene ontology: Tool for the unification
676 of biology. *Nature Genetics* 25, 25–29.

677 von Bartheld, C.S., Bahney, J., and Herculano-Houzel, S. (2016). The search for true
678 numbers of neurons and glial cells in the human brain: A review of 150 years of cell
679 counting. *Journal of Comparative Neurology* 524, 3865–3895.

680 Biswas, S., Cottarelli, A., and Agalliu, D. (2020). Neuronal and glial regulation of CNS
681 angiogenesis and barrierogenesis. *Development (Cambridge)* 147.

682 Block, M.L., Zecca, L., and Hong, J.S. (2007). Microglia-mediated neurotoxicity:
683 Uncovering the molecular mechanisms. *Nature Reviews Neuroscience* 8, 57–69.

684 Boche, D., Gerhard, A., and Rodriguez-Vieitez, E. (2019). Prospects and challenges of
685 imaging neuroinflammation beyond TSPO in Alzheimer's disease. *European Journal of*
686 *Nuclear Medicine and Molecular Imaging* 46, 2831–2847.

- 687 Bose, R., Banerjee, S., and Dunbar, G.L. (2021). Modeling Neurological Disorders in 3D
688 Organoids Using Human-Derived Pluripotent Stem Cells. *Frontiers in Cell and*
689 *Developmental Biology* 9.
- 690 Brás, J.P., Bravo, J., Freitas, J., Barbosa, M.A., Santos, S.G., Summavielle, T., and
691 Almeida, M.I. (2020). TNF-alpha-induced microglia activation requires miR-342: impact
692 on NF-kB signaling and neurotoxicity. *Cell Death and Disease* 11.
- 693 Carroll, W.M. (2019). The global burden of neurological disorders. *The Lancet Neurology*
694 18, 418–419.
- 695 Cereda, C., Baiocchi, C., Bongioanni, P., Cova, E., Guareschi, S., Metelli, M.R., Rossi,
696 B., Sbalsi, I., Cuccia, M.C., and Ceroni, M. (2008). TNF and sTNFR1/2 plasma levels in
697 ALS patients. *Journal of Neuroimmunology* 194, 123–131.
- 698 Cheng, Y., Desse, S., Martinez, A., Worthen, R.J., Jope, R.S., and Beurel, E. (2018).
699 TNF α disrupts blood brain barrier integrity to maintain prolonged depressive-like behavior
700 in mice. *Brain, Behavior, and Immunity* 69, 556–567.
- 701 Cooper, J.A. (2013). Mechanisms of cell migration in the nervous system. *Journal of Cell*
702 *Biology* 202, 725–734.
- 703 Crotti, A., and Ransohoff, R.M. (2016). Microglial Physiology and Pathophysiology:
704 Insights from Genome-wide Transcriptional Profiling. *Immunity* 44, 505–515.
- 705 Cucullo, L., Hossain, M., Puvenna, V., Marchi, N., and Janigro, D. (2011). The role of
706 shear stress in Blood-Brain Barrier endothelial physiology. *BMC Neuroscience* 12.
- 707 Cunningham, A.J., Murray, C.A., O'Neill, L.A.J., Lynch, M.A., and O'Connor, J.J. (1996).
708 Interleukin-1 β (IL-1 β) and tumour necrosis factor (TNF) inhibit long-term potentiation in
709 the rat dentate gyrus in vitro. *Neuroscience Letters* 203, 17–20.
- 710 Cunningham, C., Champion, S., Lunnon, K., Murray, C.L., Woods, J.F.C., Deacon, R.M.J.,
711 Rawlins, J.N.P., and Perry, V.H. (2009). Systemic Inflammation Induces Acute Behavioral
712 and Cognitive Changes and Accelerates Neurodegenerative Disease. *Biological*
713 *Psychiatry* 65, 304–312.
- 714 Dolmetsch, R., and Geschwind, D.H. (2011). The human brain in a dish: The promise of
715 iPSC-derived neurons. *Cell* 145, 831–834.
- 716 Erickson, M.A., and Banks, W.A. (2018). Neuroimmune axes of the blood-brain barriers
717 and blood-brain interfaces: Bases for physiological regulation, disease states, and
718 pharmacological interventions. *Pharmacological Reviews* 70, 278–314.
- 719 Ferrara, G., Errede, M., Girolamo, F., Morando, S., Ivaldi, F., Panini, N., Bendotti, C.,
720 Perris, R., Furlan, R., Virgintino, D., et al. (2016). NG2, a common denominator for
721 neuroinflammation, blood–brain barrier alteration, and oligodendrocyte precursor
722 response in EAE, plays a role in dendritic cell activation. *Acta Neuropathologica* 132, 23–
723 42.
- 724 Ferrer-Ferrer, M., and Dityatev, A. (2018). Shaping synapses by the neural extracellular
725 matrix. *Frontiers in Neuroanatomy* 12.
- 726 Franzén, B., Duvefelt, K., Jonsson, C., Engelhardt, B., Ottervald, J., Wickman, M., Yang,
727 Y., and Schuppe-Koistinen, I. (2003). Gene and protein expression profiling of human
728 cerebral endothelial cells activated with tumor necrosis factor- α . *Molecular Brain*
729 *Research* 115, 130–146.
- 730 Freitas-Andrade, M., Raman-Nair, J., and Lacoste, B. (2020). Structural and Functional
731 Remodeling of the Brain Vasculature Following Stroke. *Frontiers in Physiology* 11.

732 Frugier, T., Morganti-Kossmann, M.C., O'Reilly, D., and McLean, C.A. (2010). In situ
733 detection of inflammatory mediators in post mortem human brain tissue after traumatic
734 injury. *Journal of Neurotrauma* 27, 497–507.

735 González, H., Elgueta, D., Montoya, A., and Pacheco, R. (2014). Neuroimmune
736 regulation of microglial activity involved in neuroinflammation and neurodegenerative
737 diseases. *Journal of Neuroimmunology* 274, 1–13.

738 Gutierrez, E.G., Banks, W.A., and Kastin, A.J. (1993). Murine tumor necrosis factor alpha
739 is transported from blood to brain in the mouse. *Journal of Neuroimmunology* 47, 169–
740 176.

741 Guzman-Martinez, L., Maccioni, R.B., Andrade, V., Navarrete, L.P., Pastor, M.G., and
742 Ramos-Escobar, N. (2019a). Neuroinflammation as a common feature of
743 neurodegenerative disorders. *Frontiers in Pharmacology* 10.

744 Guzman-Martinez, L., Maccioni, R.B., Andrade, V., Navarrete, L.P., Pastor, M.G., and
745 Ramos-Escobar, N. (2019b). Neuroinflammation as a common feature of
746 neurodegenerative disorders. *Frontiers in Pharmacology* 10.

747 Haruwaka, K., Ikegami, A., Tachibana, Y., Ohno, N., Konishi, H., Hashimoto, A.,
748 Matsumoto, M., Kato, D., Ono, R., Kiyama, H., et al. (2019a). Dual microglia effects on
749 blood brain barrier permeability induced by systemic inflammation. *Nature*
750 *Communications* 10.

751 Haruwaka, K., Ikegami, A., Tachibana, Y., Ohno, N., Konishi, H., Hashimoto, A.,
752 Matsumoto, M., Kato, D., Ono, R., Kiyama, H., et al. (2019b). Dual microglia effects on
753 blood brain barrier permeability induced by systemic inflammation. *Nature*
754 *Communications* 10.

755 Heneka, M.T., and O'Banion, M.K. (2007). Inflammatory processes in Alzheimer's
756 disease. *Journal of Neuroimmunology* 184, 69–91.

757 Henry, C.J., Huang, Y., Wynne, A., Hanke, M., Himler, J., Bailey, M.T., Sheridan, J.F.,
758 and Godbout, J.P. (2008). Minocycline attenuates lipopolysaccharide (LPS)-induced
759 neuroinflammation, sickness behavior, and anhedonia. *Journal of Neuroinflammation* 5.

760 Hesari, Z., Soleimani, M., Atyabi, F., Sharifdini, M., Nadri, S., Warkiani, M.E., Zare, M.,
761 and Dinarvand, R. (2016). A hybrid microfluidic system for regulation of neural
762 differentiation in induced pluripotent stem cells. *Journal of Biomedical Materials Research*
763 *- Part A* 104, 1534–1543.

764 Horng, S., Therattil, A., Moyon, S., Gordon, A., Kim, K., Argaw, A.T., Hara, Y., Mariani,
765 J.N., Sawai, S., Flodby, P., et al. (2017). Astrocytic tight junctions control inflammatory
766 CNS lesion pathogenesis. *Journal of Clinical Investigation* 127, 3136–3151.

767 Huh, D., Kim, H.J., Fraser, J.P., Shea, D.E., Khan, M., Bahinski, A., Hamilton, G.A., and
768 Ingber, D.E. (2013). Microfabrication of human organs-on-chips. *Nature Protocols* 8,
769 2135–2157.

770 Jiang, H., Hampel, H., Prvulovic, D., Wallin, A., Blennow, K., Li, R., and Shen, Y. (2011).
771 Elevated CSF levels of TACE activity and soluble TNF receptors in subjects with mild
772 cognitive impairment and patients with Alzheimer's disease. *Molecular*
773 *Neurodegeneration* 6.

774 Jones, A.R., and Shusta, E. V. (2007). Blood-brain barrier transport of therapeutics via
775 receptor-mediation. *Pharmaceutical Research* 24, 1759–1771.

776 Keaney, J., and Campbell, M. (2015). The dynamic blood-brain barrier. *FEBS Journal*
777 282, 4067–4079.

778 Kim, Y.S., and Joh, T.H. (2006). Microglia, major player in the brain inflammation: Their
779 roles in the pathogenesis of Parkinson's disease. *Experimental and Molecular Medicine*
780 *38*, 333–347.

781 Kouchaki, E., Kakhaki, R.D., Tamtaji, O.R., Dadgostar, E., Behnam, M., Nikoueinejad, H.,
782 and Akbari, H. (2018). Increased serum levels of TNF- α and decreased serum levels of
783 IL-27 in patients with Parkinson disease and their correlation with disease severity.
784 *Clinical Neurology and Neurosurgery* *166*, 76–79.

785 Kuno, R., Wang, J., Kawanokuchi, J., Takeuchi, H., Mizuno, T., and Suzumura, A. (2005).
786 Autocrine activation of microglia by tumor necrosis factor- α . *Journal of Neuroimmunology*
787 *162*, 89–96.

788 Lam, D., Enright, H.A., Cadena, J., Peters, S.K.G., Sales, A.P., Osburn, J.J., Soscia, D.A.,
789 Kulp, K.S., Wheeler, E.K., and Fischer, N.O. (2019). Tissue-specific extracellular matrix
790 accelerates the formation of neural networks and communities in a neuron-glia co-culture
791 on a multi-electrode array. *Scientific Reports* *9*.

792 Lau, L.T., and Yu, A.C.H. (2001). Astrocytes produce and release interleukin-1,
793 interleukin-6, tumor necrosis factor alpha and interferon-gamma following traumatic and
794 metabolic injury. *Journal of Neurotrauma* *18*, 351–359.

795 Liddelow, S.A., and Barres, B.A. (2017). Reactive Astrocytes: Production, Function, and
796 Therapeutic Potential. *Immunity* *46*, 957–967.

797 Liddelow, S.A., Guttenplan, K.A., Clarke, L.E., Bennett, F.C., Bohlen, C.J., Schirmer, L.,
798 Bennett, M.L., Münch, A.E., Chung, W.S., Peterson, T.C., et al. (2017). Neurotoxic
799 reactive astrocytes are induced by activated microglia. *Nature* *541*, 481–487.

800 Liebner, S., Dijkhuizen, R.M., Reiss, Y., Plate, K.H., Agalliu, D., and Constantin, G.
801 (2018). Functional morphology of the blood–brain barrier in health and disease. *Acta*
802 *Neuropathologica* *135*, 311–336.

803 Linnerbauer, M., Wheeler, M.A., and Quintana, F.J. (2020). Astrocyte Crosstalk in CNS
804 Inflammation. *Neuron* *108*, 608–622.

805 Lonsdale, J., Thomas, J., Salvatore, M., Phillips, R., Lo, E., Shad, S., Hasz, R., Walters,
806 G., Garcia, F., Young, N., et al. (2013). The Genotype-Tissue Expression (GTEx) project.
807 *Nature Genetics* *45*, 580–585.

808 Love, M.I., Huber, W., and Anders, S. (2014). Moderated estimation of fold change and
809 dispersion for RNA-seq data with DESeq2. *Genome Biology* *15*.

810 Manatakis, D. v, VanDevender, A., and Manolakos, E.S. (2020). An information-theoretic
811 approach for measuring the distance of organ tissue samples using their transcriptomic
812 signatures. *Bioinformatics*.

813 Maoz, B.M., Herland, A., Fitzgerald, E.A., Grevesse, T., Vidoudez, C., Pacheco, A.R.,
814 Sheehy, S.P., Park, T.E., Dauth, S., Mannix, R., et al. (2018). A linked organ-on-chip
815 model of the human neurovascular unit reveals the metabolic coupling of endothelial and
816 neuronal cells. *Nature Biotechnology* *36*, 865–877.

817 Marchetti, L., and Engelhardt, B. (2020). Immune cell trafficking across the blood-brain
818 barrier in the absence and presence of neuroinflammation. *Vascular Biology* *2*, H1–H18.

819 McConnell, H.L., Kersch, C.N., Woltjer, R.L., and Neuwelt, E.A. (2017). The translational
820 significance of the neurovascular unit. *Journal of Biological Chemistry* *292*, 762–770.

821 Merlini, M., Rafalski, V.A., Ma, K., Kim, K.Y., Bushong, E.A., Rios Coronado, P.E., Yan,
822 Z., Mendiola, A.S., Sozmen, E.G., Ryu, J.K., et al. (2021). Microglial Gi-dependent
823 dynamics regulate brain network hyperexcitability. *Nature Neuroscience* *24*, 19–23.

824 Mi, H., Muruganujan, A., Casagrande, J.T., and Thomas, P.D. (2013). Large-scale gene
825 function analysis with the panther classification system. *Nature Protocols* 8, 1551–1566.
826 Minghetti, L. (2005). Role of inflammation in neurodegenerative diseases. *Current*
827 *Opinion in Neurology*.
828 Muoio, V., Persson, P.B., and Sendeski, M.M. (2014). The neurovascular unit - concept
829 review. *Acta Physiologica* 210, 790–798.
830 Neniskyte, U., Vilalta, A., and Brown, G.C. (2014a). Tumour necrosis factor alpha-induced
831 neuronal loss is mediated by microglial phagocytosis. *FEBS Letters* 588, 2952–2956.
832 Neniskyte, U., Vilalta, A., and Brown, G.C. (2014b). Tumour necrosis factor alpha-induced
833 neuronal loss is mediated by microglial phagocytosis. *FEBS Letters* 588, 2952–2956.
834 Nishioku, T., Matsumoto, J., Dohgu, S., Sumi, N., Miyao, K., Takata, F., Shuto, H.,
835 Yamauchi, A., and Kataoka, Y. (2010). Tumor necrosis factor- α mediates the blood-brain
836 barrier dysfunction induced by activated microglia in mouse brain microvascular
837 endothelial cells. *Journal of Pharmacological Sciences* 112, 251–254.
838 Obermeier, B., Daneman, R., and Ransohoff, R.M. (2013). Development, maintenance
839 and disruption of the blood-brain barrier. *Nature Medicine* 19, 1584–1596.
840 Olmos, G., and Lladó, J. (2014). Tumor necrosis factor alpha: A link between
841 neuroinflammation and excitotoxicity. *Mediators of Inflammation* 2014.
842 Osburg, B., Peiser, C., Dömling, D., Schomburg, L., Ko, Y.T., Voigt, K., and Bickel, U.
843 (2002). Effect of endotoxin on expression of TNF receptors and transport of TNF- α at the
844 blood-brain barrier of the rat. *American Journal of Physiology - Endocrinology and*
845 *Metabolism* 283.
846 Pan, W., and Kastin, A.J. (2002). TNF α transport across the blood-brain barrier is
847 abolished in receptor knockout mice. *Experimental Neurology* 174, 193–200.
848 Pan, W., and Kastin, A.J. (2007). Tumor necrosis factor and stroke: Role of the blood-
849 brain barrier. *Progress in Neurobiology* 83, 363–374.
850 Pan, W., Banks, W.A., and Kastin, A.J. (1997). Permeability of the blood-brain and blood-
851 spinal cord barriers to interferons. *Journal of Neuroimmunology* 76, 105–111.
852 Pan, W., Zhang, L., Liao, J., Csernus, B., and Kastin, A.J. (2003a). Selective increase in
853 TNF α permeation across the blood-spinal cord barrier after SCI. *Journal of*
854 *Neuroimmunology* 134, 111–117.
855 Pan, W., Csernus, B., and Kastin, A.J. (2003b). Upregulation of p55 and p75 Receptors
856 Mediating TNF- α Transport Across the Injured Blood-Spinal Cord Barrier. *Journal of*
857 *Molecular Neuroscience* 21, 173–184.
858 Park, T.E., Mustafaoglu, N., Herland, A., Hasselkus, R., Mannix, R., FitzGerald, E.A.,
859 Prantil-Baun, R., Watters, A., Henry, O., Benz, M., et al. (2019). Hypoxia-enhanced
860 Blood-Brain Barrier Chip recapitulates human barrier function and shuttling of drugs and
861 antibodies. *Nature Communications* 10.
862 Pediaditakis, I., Kodella, K.R., Manatakis, D. v., Le, C.Y., Hinojosa, C.D., Tien-Street, W.,
863 Manolagos, E.S., Vekrellis, K., Hamilton, G.A., Ewart, L., et al. (2021). Modeling alpha-
864 synuclein pathology in a human brain-chip to assess blood-brain barrier disruption.
865 *Nature Communications* 12.
866 Perry, V.H. (2004). The influence of systemic inflammation on inflammation in the brain:
867 Implications for chronic neurodegenerative disease. *Brain, Behavior, and Immunity* 18,
868 407–413.

- 869 Perry, V.H., Cunningham, C., and Holmes, C. (2007a). Systemic infections and
870 inflammation affect chronic neurodegeneration. *Nature Reviews Immunology* 7, 161–167.
- 871 Perry, V.H., Cunningham, C., and Holmes, C. (2007b). Systemic infections and
872 inflammation affect chronic neurodegeneration. *Nature Reviews Immunology* 7, 161–167.
- 873 Perry, V.H., Nicoll, J.A.R., and Holmes, C. (2010). Microglia in neurodegenerative
874 disease. *Nature Reviews Neurology* 6, 193–201.
- 875 Qian, T., Maguire, S.E., Canfield, S.G., Bao, X., Olson, W.R., Shusta, E. V., and Palecek,
876 S.P. (2017). Directed differentiation of human pluripotent stem cells to blood-brain barrier
877 endothelial cells. *Science Advances* 3, e1701679.
- 878 Qin, L., Wu, X., Block, M.L., Liu, Y., Breese, G.R., Hong, J.S., Knapp, D.J., and Crews,
879 F.T. (2007). Systemic LPS causes chronic neuroinflammation and progressive
880 neurodegeneration. *GLIA* 55, 453–462.
- 881 Rakic, P. (1990). Principles of neural cell migration. *Experientia* 46, 882–891.
- 882 Ritchie, M.E., Phipson, B., Wu, D., Hu, Y., Law, C.W., Shi, W., and Smyth, G.K. (2015).
883 Limma powers differential expression analyses for RNA-sequencing and microarray
884 studies. *Nucleic Acids Research* 43, e47.
- 885 Rochfort, K.D., Collins, L.E., Murphy, R.P., and Cummins, P.M. (2014). Downregulation
886 of blood-brain barrier phenotype by proinflammatory cytokines involves NADPH oxidase-
887 dependent ROS generation: Consequences for interendothelial adherens and tight
888 junctions. *PLoS ONE* 9.
- 889 Rochfort, K.D., Collins, L.E., McLoughlin, A., and Cummins, P.M. (2016). Tumour
890 necrosis factor- α -mediated disruption of cerebrovascular endothelial barrier integrity in
891 vitro involves the production of proinflammatory interleukin-6. *Journal of Neurochemistry*
892 136, 564–572.
- 893 Rossi, S., Motta, C., Studer, V., Barbieri, F., Buttari, F., Bergami, A., Sancesario, G.,
894 Bernardini, S., De Angelis, G., Martino, G., et al. (2014). Tumor necrosis factor is elevated
895 in progressive multiple sclerosis and causes excitotoxic neurodegeneration. *Multiple*
896 *Sclerosis Journal* 20, 304–312.
- 897 Rothhammer, V., and Quintana, F.J. (2015). Control of autoimmune CNS inflammation
898 by astrocytes. *Seminars in Immunopathology* 37, 625–638.
- 899 Ryu, J.K., and McLarnon, J.G. (2006). Minocycline or iNOS inhibition block 3-nitrotyrosine
900 increases and blood-brain barrier leakiness in amyloid beta-peptide-injected rat
901 hippocampus. *Experimental Neurology* 198, 552–557.
- 902 Sances, S., Ho, R., Vatine, G., West, D., Laperle, A., Meyer, A., Godoy, M., Kay, P.S.,
903 Mandefro, B., Hatata, S., et al. (2018). Human iPSC-Derived Endothelial Cells and
904 Microengineered Organ-Chip Enhance Neuronal Development. *Stem Cell Reports* 10,
905 1222–1236.
- 906 Shepro, D., and Morel, N.M.L. (1993). Pericyte physiology. *The FASEB Journal* 7, 1031–
907 1038.
- 908 Shi, L., Zeng, M., Sun, Y., and Fu, B.M. (2014). Quantification of blood-brain barrier solute
909 permeability and brain transport by multiphoton microscopy. *Journal of Biomechanical*
910 *Engineering* 136.
- 911 Singh, A., Jones, O.D., Mockett, B.G., Ohline, S.M., and Abraham, W.C. (2019). Tumor
912 Necrosis Factor- α -Mediated Metaplastic Inhibition of LTP Is Constitutively Engaged in an
913 Alzheimer's Disease Model. *The Journal of Neuroscience : The Official Journal of the*
914 *Society for Neuroscience* 39, 9083–9097.

- 915 Sofroniew, M. V. (2015). Astrocyte barriers to neurotoxic inflammation. *Nature Reviews*
916 *Neuroscience* *16*, 249–263.
- 917 Sofroniew, M. V. (2020). Astrocyte Reactivity: Subtypes, States, and Functions in CNS
918 Innate Immunity. *Trends in Immunology* *41*, 758–770.
- 919 Stone, N.L., England, T.J., and O'Sullivan, S.E. (2019). A novel transwell blood brain
920 barrier model using primary human cells. *Frontiers in Cellular Neuroscience* *13*.
- 921 Streit, W.J., and Kincaid-Colton, C.A. (1995). The brain's immune system. *Scientific*
922 *American* *273*.
- 923 Sultan, K.T., and Shi, S.H. (2018). Generation of diverse cortical inhibitory interneurons.
924 *Wiley Interdisciplinary Reviews: Developmental Biology* *7*.
- 925 Sun, J., Zheng, J.H., Zhao, M., Lee, S., and Goldstein, H. (2008). Increased In Vivo
926 Activation of Microglia and Astrocytes in the Brains of Mice Transgenic for an Infectious
927 R5 Human Immunodeficiency Virus Type 1 Provirus and for CD4-Specific Expression of
928 Human Cyclin T1 in Response to Stimulation by Lipopolysaccharides. *Journal of Virology*
929 *82*, 5562–5572.
- 930 Sweeney, M.D., Zhao, Z., Montagne, A., Nelson, A.R., and Zlokovic, B. V. (2019). Blood-
931 brain barrier: From physiology to disease and back. *Physiological Reviews* *99*, 21–78.
- 932 Tangpong, J., Cole, M.P., Sultana, R., Joshi, G., Estus, S., Vore, M., St. Clair, W.,
933 Ratanachaiyavong, S., St. Clair, D.K., and Butterfield, D.A. (2006). Adriamycin-induced,
934 TNF- α -mediated central nervous system toxicity. *Neurobiology of Disease* *23*, 127–139.
- 935 Thomsen, L.B., Burkhardt, A., and Moos, T. (2015). A triple culture model of the blood-
936 brain barrier using porcine brain endothelial cells, astrocytes and pericytes. *PLoS ONE*
937 *10*.
- 938 Trickler, W.J., Mayhan, W.G., and Miller, D.W. (2005). Brain microvessel endothelial cell
939 responses to tumor necrosis factor-alpha involve a nuclear factor kappa B (NF- κ B) signal
940 transduction pathway. *Brain Research* *1048*, 24–31.
- 941 Uhlén, M., Fagerberg, L., Hallström, B.M., Lindskog, C., Oksvold, P., Mardinoglu, A.,
942 Sivertsson, Å., Kampf, C., Sjöstedt, E., Asplund, A., et al. (2015). Tissue-based map of
943 the human proteome. *Science* *347*.
- 944 Vatine, G.D., Barrile, R., Workman, M.J., Sances, S., Barriga, B.K., Rahnama, M.,
945 Barthakur, S., Kasendra, M., Lucchesi, C., Kerns, J., et al. (2019). Human iPSC-Derived
946 Blood-Brain Barrier Chips Enable Disease Modeling and Personalized Medicine
947 Applications. *Cell Stem Cell* *24*, 995-1005.e6.
- 948 Verma, S., Nakaoke, R., Dohgu, S., and Banks, W.A. (2006). Release of cytokines by
949 brain endothelial cells: A polarized response to lipopolysaccharide. *Brain, Behavior, and*
950 *Immunity* *20*, 449–455.
- 951 Veys, K., Fan, Z., Ghobrial, M., Bouché, A., García-Caballero, M., Vriens, K., Conchinha,
952 N.V., Seuwen, A., Schlegel, F., Gorski, T., et al. (2020). Role of the GLUT1 Glucose
953 Transporter in Postnatal CNS Angiogenesis and Blood-Brain Barrier Integrity. *Circulation*
954 *Research* *127*, 466–482.
- 955 De Vries, H.E., Blom-Roosemalen, M.C.M., Van Oosten, M., De Boer, A.G., Van Berkel,
956 T.J.C., Breimer, D.D., and Kuiper, J. (1996). The influence of cytokines on the integrity of
957 the blood-brain barrier in vitro. *Journal of Neuroimmunology* *64*, 37–43.
- 958 Wang, W.Y., Tan, M.S., Yu, J.T., and Tan, L. (2015). Role of pro-inflammatory cytokines
959 released from microglia in Alzheimer's disease. *Annals of Translational Medicine* *3*.

960 Wong, A.D., Ye, M., Levy, A.F., Rothstein, J.D., Bergles, D.E., and Searson, P.C. (2013).
961 The blood-brain barrier: An engineering perspective. *Frontiers in Neuroengineering* 6.
962 Xu, X., Roby, K.D., and Callaway, E.M. (2010). Immunochemical characterization of
963 inhibitory mouse cortical neurons: Three chemically distinct classes of inhibitory cells.
964 *Journal of Comparative Neurology* 518, 389–404.
965 Yang, Y., Salayandia, V.M., Thompson, J.F., Yang, L.Y., Estrada, E.Y., and Yang, Y.
966 (2015). Attenuation of acute stroke injury in rat brain by minocycline promotes blood-brain
967 barrier remodeling and alternative microglia/macrophage activation during recovery.
968 *Journal of Neuroinflammation* 12.
969 Yarlagadda, A., Alfson, E., and Clayton, A.H. (2009). The blood brain barrier and the role
970 of cytokines in neuropsychiatry. *Psychiatry* 6, 18–22.
971 Ye, L., Huang, Y., Zhao, L., Li, Y., Sun, L., Zhou, Y., Qian, G., and Zheng, J.C. (2013).
972 IL-1 β and TNF- α induce neurotoxicity through glutamate production: A potential role for
973 neuronal glutaminase. *Journal of Neurochemistry* 125, 897–908.
974 Yenari, M.A., Xu, L., Xian, N.T., Qiao, Y., and Giffard, R.G. (2006). Microglia potentiate
975 damage to blood-brain barrier constituents: Improvement by minocycline in vivo and in
976 vitro. *Stroke* 37, 1087–1093.
977 Yin, X., Mead, B.E., Safaee, H., Langer, R., Karp, J.M., and Levy, O. (2016). Engineering
978 Stem Cell Organoids. *Cell Stem Cell* 18, 25–38.
979 Yuan, W., Lv, Y., Zeng, M., and Fu, B.M. (2009). Non-invasive measurement of solute
980 permeability in cerebral microvessels of the rat. *Microvascular Research* 77, 166–173.
981 Zaremba, J., and Losy, J. (2001). Early TNF- α levels correlate with ischaemic stroke
982 severity. *Acta Neurologica Scandinavica* 104, 288–295.
983 Zhao, C., Ling, Z., Newman, M.B., Bhatia, A., and Carvey, P.M. (2007). TNF- α knockout
984 and minocycline treatment attenuates blood-brain barrier leakage in MPTP-treated mice.
985 *Neurobiology of Disease* 26, 36–46.
986
987
988
989
990
991
992
993
994
995
996
997
998
999
1000
1001
1002
1003
1004
1005

1006 **AUTHOR CONTRIBUTION**

1007 I.P. developed the Brain-Chip model, designed, and performed experiments, collected,
1008 and analyzed data, and wrote the paper. K.R.K. contributed to the Brain-Chip model
1009 development, performed experiments, collected data, and contributed to the writing of the
1010 paper. D.V.M. processed and analyzed the transcriptomic data, incorporated the
1011 associated data in the manuscript and contributed to the writing of the paper. C.Y.L, S.B.
1012 and A.S. helped perform experiments. E.S.M. was involved in the bioinformatic analysis
1013 and contributed to the writing of the paper. A.G., L.E., L.L.R provided critical feedback
1014 and reviewed the manuscript. C.D.H. provided insightful input on the engineering aspects
1015 of the project. K.K. supervised the project, contributed to the Brain-Chip model
1016 development, and wrote the paper.

1017
1018 **ACKNOWLEDGMENTS**

1019 We would like to thank Dr. Athanasia Apostolou for providing technical assistance with
1020 the scanning electron microscope. This work was supported by the National Institute of
1021 Health, National Center for Advancing Translational Sciences (UG3TR002188; to C.D.H.
1022 and K.K.). The content is solely the responsibility of the authors and does not necessarily
1023 represent the official views of the National Institutes of Health. We also thank Brett Clair
1024 for scientific illustrations.

1025
1026 **CONFLICT OF INTEREST**

1027 I.P., K.R.K., D.V.M., C.Y.L, S.B., A.S., L.E., C.D.H., and K.K. are current or former
1028 employees of Emulate, Inc and may hold equity interests in Emulate, Inc. All other authors
1029 declare no competing interests.

1030
1031
1032
1033
1034
1035
1036
1037
1038
1039
1040
1041
1042
1043
1044
1045
1046
1047
1048
1049
1050
1051

1052 **FIGURE LEGENDS**

1053 **Figure 1. Reconstruction of the neurovascular unit in the Brain-Chip**

1054 (A) Schematic illustration of the Brain-Chip, a two-channel micro-engineered chip
1055 including iPSC-derived brain endothelial-like cells cultured on all surfaces of the bottom
1056 channel, and iPSC-derived Glutamatergic and GABAergic neurons, primary human brain
1057 astrocytes, pericytes, and microglia on the surface of the top channel.

1058 (B) Confocal images of the cell coverage in the brain channel on day 7 of culture. Top
1059 image: Immunofluorescence staining of the brain channel including MAP2 (green), GFAP
1060 (magenta), NG2 (red), and DAPI (blue). Bottom images: Representative merged confocal
1061 image of the brain channel on culture day 7, stained for neurons (MAP2, green),
1062 astrocytes (GFAP, magenta, IBA1, yellow), and pericytes (α SMA, red) (bar, 50 μ m).

1063 (C) Representative immunofluorescent staining for s100 β (red) and GLAST (green)
1064 (bar, 100 μ m).

1065 (D) FACS analysis of cell specific markers of microglia: Total population of microglia within
1066 the brain channel (grey), CD11b positive population (magenta), CD45 positive population
1067 (magenta), quantification of CD11b:CD45 positive cells.

1068 (E) Representative merged confocal image of the brain channel co-stained with VGAT
1069 (green) for GABAergic neurons and VGLUT1 (red) for Glutamatergic neurons (bar, 100
1070 μ m).

1071 (F) Immunofluorescence staining of the brain channel including MAP2 (green), and SYP
1072 (red) (bar, 100 μ m).

1073 (G) Levels of secreted glutamate in the brain channel on culture days 5, 6 and 7 (n=4-6
1074 independent chips, ****P<0.0001, NS: not significant compared to the transwells group
1075 n=3-4). Data are expressed as mean \pm S.E.M, statistical analysis by two-way ANOVA
1076 with Tukey's multiple comparisons test.

1077

1078 **Figure 2. Characterization of the Barrier in the Brain-Chip**

1079 (A) Top Image: Immunofluorescence staining of the vascular channel stained for the tight
1080 junction marker ZO-1 (green) (bar, 1 mm). Bottom Images: Immunofluorescence
1081 micrographs of the human brain endothelium cultured on-chip for 7 days labeled with
1082 Occludin (green), PECAM1 (magenta), and DAPI (blue) (bar, 100 μ m).

1083 (B) Quantitative barrier function analysis by the apparent permeability to 3kDa fluorescent
1084 dextran, in two independent iPSC donor lines on culture days 5, 6, and 7 (n=4-6
1085 independent chips). NS: not significant. Data are expressed as mean \pm S.E.M., statistical
1086 analysis by Student's t-test.

1087 (C) The apparent permeability of different size dextran molecules (3-70 kDa) across
1088 Brain-Chips correlated with previously reported *in vivo* rodent brain uptake data. (n=3-5
1089 independent chips). Data are expressed as mean \pm S.E.M.)

1090 (D) Left: Exploded view of the chip. Interaction of primary human astrocyte end-feet-like
1091 processes (GFAP, red) with endothelial-like cells (ZO-1, yellow), MAP2 (green). Right:
1092 Representative Scanning Electron Microscopy (SEM) image showing astrocytic endfoot
1093 passing through 7 μ m pores into the vascular channel (bar, 30 μ m). White arrows show
1094 the astrocytic endfoot.

1095

1096 **Figure 3. Comparative analyses of the transcriptomic profiles of the Brain-Chip,**
1097 **adult cortex tissue and transwell culture**

1098 (A) Principal Component Analysis (PCA) of RNAseq data from the brain channel of the
1099 Brain-Chip and the transwell brain cells culture on culture days 5 and 7 (n=4 per
1100 condition). The first two PCs explain the 47.47% of the total variance.
1101 (B) DGE analysis Identified up (cyan) - and down (magenta) - regulated genes (dots) in
1102 the Brain-Chip as compared to transwells on culture day 7.
1103 (C to D) Biological processes in Brain-Chip and transwells, as identified by Gene Ontology
1104 (GO) enrichment analysis based on the DE genes.
1105 (E) Boxplots summarizing the distributions of the corresponding pairwise TSD distances.
1106 In each pair, one sample belongs to the reference tissue (Human Brain-Cortex) and the
1107 other either to the reference tissue or to one of our culture models, i.e., Brain-Chip or
1108 transwell, from culture days 5 and 7. The Brain-Chip and transwell cultures were run in
1109 parallel. n=4 independent chips; data are expressed as mean \pm S.E.M. NS: Not
1110 Significant, **P<0.01, ***P<0.001; statistical analysis with two-sample t-test using a null
1111 hypothesis that the data from human tissue and the data from chips or transwells comes
1112 from independent random samples from normal distributions with equal means and equal
1113 but unknown variances. On each box the red line indicates the median and the bottom
1114 and top edges correspond to the 25th and 75th percentiles respectively. The whiskers
1115 extend to the most extreme but not considered outliers values.
1116

1117 **Figure 4. Response of the Brain-Chip to neuroinflammation**

1118 (A) Schematic illustration of the induction of neuroinflammation by perfusion of TNF- α
1119 through the brain channel.
1120 (B to D) Secreted levels of IL-1 β , IL-6, and IFN γ in control or TNF- α -treated Brain-Chips
1121 including, or not, microglia and/or astrocytes. n=4-5 independent chips; data are
1122 expressed as mean \pm S.E.M. NS: Not Significant, *P<0.05, **P<0.01, ****P<0.0001;
1123 statistical analysis with Student's t-test.
1124 (E to F) Representative immunofluorescent staining for microglia (CD68, red), neurons
1125 (MAP2, green), astrocytes (GFAP, magenta), and nuclei (DAPI, blue) in TNF- α -treated of
1126 control chips (bar, 100 nm).
1127 (G) Quantification of the CD68-positive events/field of view in 4 randomly selected
1128 different areas/chip, n=3 Brain-Chips; data are expressed as mean \pm S.E.M., **P<0.01
1129 compared to the untreated control group, statistical analysis by Student's t-test.
1130 (H) Quantification of the number of GFAP-positive and MAP2 events/field of view in n=4
1131 randomly selected different areas/chip, n=3 Brain-Chips, **P<0.01, compared to the
1132 untreated control group; statistical analysis with Student's t-test.
1133 (I) Immunofluorescence images show an example of the two types of astrocyte
1134 morphology in cultures (polygonal shape towards more elongated shape), after
1135 immunostaining with an antibody against GFAP (bar, 100 nm).
1136 (J) Representative immunofluorescent staining for pericytes (NG2, red) in TNF- α -treated
1137 or control chips (bar, 100 nm).
1138 (K) Quantification of NG2 fluorescent intensity in n=5 randomly selected different
1139 areas/chip, n=3 Brain-Chips; data are expressed as mean \pm S.E.M., ****P<0.0001
1140 compared to the untreated control group; statistical analysis with Student's t-test.
1141 (L) Quantification of the number of MAP2 events/field of view in n=4 randomly selected
1142 different areas/chip, n=3 Brain-Chips, ****P<0.0001, compared to the untreated control
1143 group; statistical analysis with Student's t-test.

1144 (M) Levels of secreted glutamate in the brain channel on culture day 7 (n=6-7 independent
1145 chips. **** $P < 0.0001$, compared to the untreated group. Data are expressed as mean \pm
1146 S.E.M, statistical analysis by Student's t-test.

1147

1148 **Figure 5. Barrier changes during neuroinflammation**

1149 (A) Representative merged image of immunofluorescent staining of Intercellular
1150 Adhesion Molecule 1 (ICAM-1, red), tight junction protein 1 (ZO-1, green), and cell nuclei
1151 (DAPI, blue), (bar, 100 nm).

1152 (B) Quantification of barrier permeability to 3 kDa fluorescent dextran, upon 24 and 48 h
1153 of treatment with TNF- α ; n=3-4 independent chips. Data are expressed as mean \pm S.E.M,
1154 NS: Not Significant, ** $P < 0.01$, control compared to TNF- α treated group; statistical
1155 analysis by two-way ANOVA followed by Tukey's multiple comparisons test.

1156 (C) Assessment of the permeability of the Brain-Chip on culture day 7, in the absence or
1157 presence of microglia, astrocytes or neurons; n=4-8 independent chips; data are
1158 expressed as mean \pm S.E.M., **** $P < 0.0001$, NS: Not Significant compared to full model
1159 (Brain-Chip), statistical analysis by one-way ANOVA with Sidak's multiple comparisons
1160 test.

1161 (D) Quantification of barrier apparent permeability to 3 kDa fluorescent dextran, upon 48
1162 h of TNF- α -treated Brain-Chips including minocycline, or not (control); n=3-5 independent
1163 chips. Data are expressed as mean \pm S.E.M, **** $P < 0.0001$, NS: Not Significant compared
1164 to TNF- α treated group or minocycline group; statistical analysis by Student's t-test.

1165

1166 **Figure 6. Brain-Chip response to TNF- α perfused through the vascular channel**

1167 (A to C) Representative immunofluorescent staining for microglia (CD68, red), neurons
1168 (MAP2, green), astrocytes (GFAP, magenta), nuclei (DAPI, blue), and pericytes (NG2,
1169 red) in TNF- α -treated of control chips (bar, 100 nm).

1170 (D) Quantification of the CD68-positive events/field of view in n=4 randomly selected
1171 different areas/chip, n=3 Brain-Chips; data are expressed as mean \pm S.E.M.,
1172 **** $P < 0.0001$ compared to the untreated control group, statistical analysis by Student's t-
1173 test.

1174 (E) (Left) Quantification of the number of GFAP-positive events/field of view in n=4
1175 randomly selected different areas/chip, n=3 Brain-Chips; data are expressed as mean \pm
1176 S.E.M., *** $P < 0.001$ compared to the untreated control group; statistical analysis with
1177 Student's t-test. (Right) Quantification of GFAP fluorescent intensity in n=3 randomly
1178 selected different areas/chip, n=3 Brain-Chips, **** $P < 0.0001$ compared to the untreated
1179 control group, statistical analysis with Student's t-test.

1180 (F) Quantification of fluorescent intensity of NG2 in, n=4, randomly selected different
1181 areas/chip, n=3 Brain-Chips; data are expressed as mean \pm S.E.M., **** $P < 0.0001$
1182 compared to the untreated control group; statistical analysis with Student's t-test.

1183 (G) The nuclei counts based on DAPI staining were similar between the control and
1184 treated groups (n=4 Brain-Chips, data are expressed as mean \pm S.E.M., NS: Not
1185 Significant compared to the untreated control group). Statistical analysis with Student's t-
1186 test.

1187 (H to J) Secreted levels of the proinflammatory cytokines IL-6, IL-1 β and IFN γ , in the
1188 brain channel of control or TNF- α treated Brain-Chips. n=3-4 independent chips, data are

1189 expressed as mean \pm S.E.M., * $P < 0.05$, $P^{**} < 0.01$, $P^{****} < 0.0001$, statistical analysis with
1190 Student's t-test.

1191 (K) Quantification of the number of MAP2 events/field of view in $n=4$ randomly selected
1192 different areas/chip, $n=3$ Brain-Chips, data are expressed as mean \pm S.E.M., NS: Not
1193 Significant compared to the untreated control group, statistical analysis with Student's t-
1194 test.

1195 (L) Levels of secreted glutamate in the brain channel on culture day 7 ($n=6$ independent
1196 chips; data are expressed as mean \pm S.E.M., NS: Not Significant compared to the
1197 untreated control group). Statistical analysis with Student's t-test.

1198 (M) Immunofluorescent staining of cell nuclei (DAPI, blue), Intercellular Adhesion
1199 Molecule 1 (ICAM-1, red), tight junction protein 1 (ZO-1, green), and a merged image of
1200 all three markers (bar, 100 nm).

1201 (N) Quantitative barrier function analysis via apparent permeability to 3kDa fluorescent
1202 dextran, upon 48h of exposure to TNF- α via the vascular channel. $n=3\sim 4$ independent
1203 chips, NS= Not Significant, * $P < 0.05$, control group compared to TNF- α treated group after
1204 24h and 48 h of treatment; data are expressed as mean \pm S.E.M, statistical analysis by
1205 two-way ANOVA with Tukey's multiple comparisons test.

1206

1207 **Figure 7. Impact of inflammation on barrier transport systems**

1208 (A, B) The transport of TNF- α from the brain to vascular or vice versa was shown by
1209 assessment of the levels of TNF- α secreted in the vascular or brain channel of control
1210 (basal levels) or TNF- α dosed chips either through the brain (brain to vascular) or the
1211 vascular channel (vascular to brain), $n=6$ independent chips, data are expressed as mean
1212 \pm S.E.M., $P^* < 0.05$, $P^{**} < 0.01$, $P^{****} < 0.0001$, statistical analysis by two-way ANOVA with
1213 Tukey's multiple comparisons test.

1214 (C) Representative immunofluorescence images of GLUT-1 transporter (red) expression
1215 and DAPI (blue), in the endothelial cells of the vascular channel of the Brain Chip upon
1216 challenge with TNF- α through the brain or the vascular channels. Vehicle-treated chips
1217 serve as control (bar, 100 nm).

1218 (D) Quantification of the GLUT-1-fluorescence intensity /field of view in 4 randomly
1219 selected different areas/chip, $n=4$ Brain-Chips; data are expressed as mean \pm S.E.M.,
1220 $P^{****} < 0.0001$ compared to the untreated control group, statistical analysis by two-way
1221 ANOVA with Tukey's multiple comparisons test.

1222

1223

1224

1225

1226

1227

1228

1229

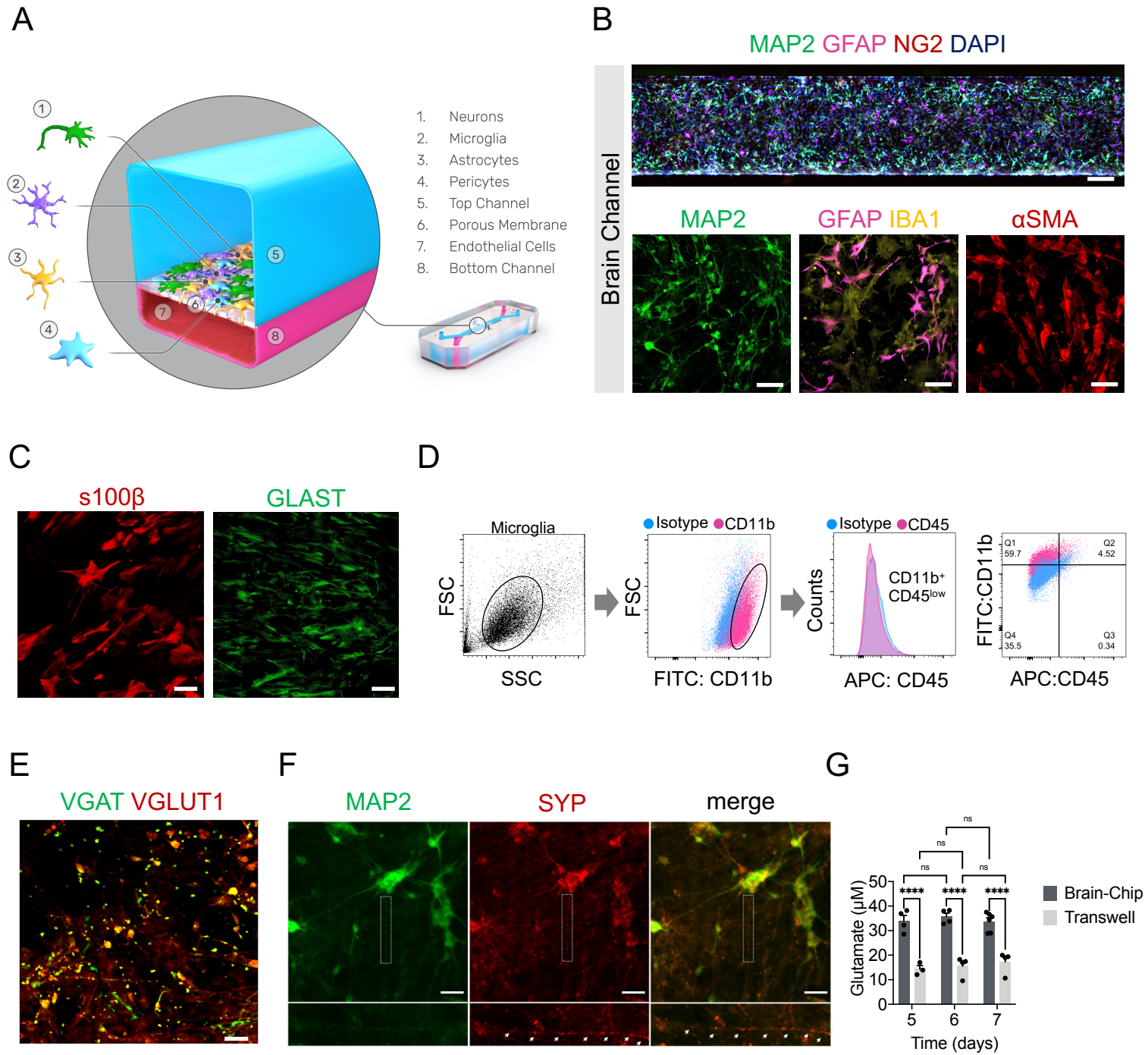
1230

1231

1232

1233

1234



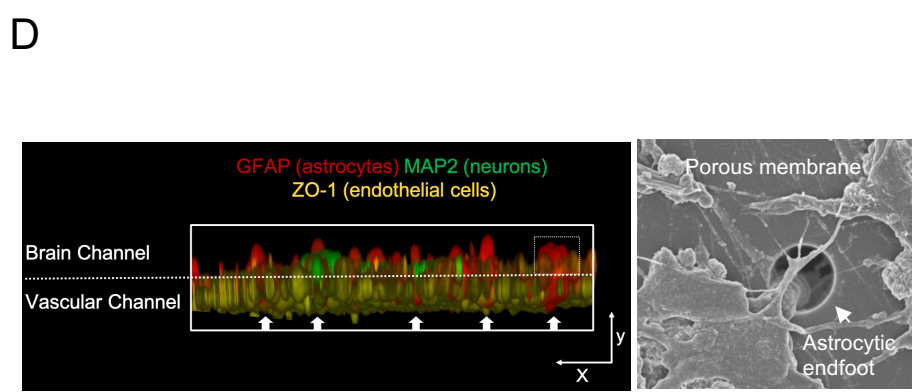
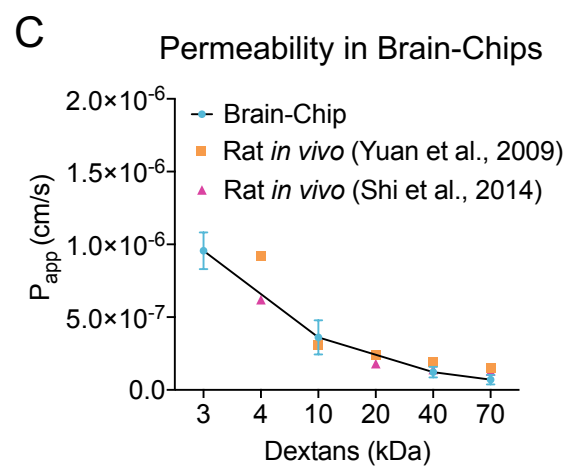
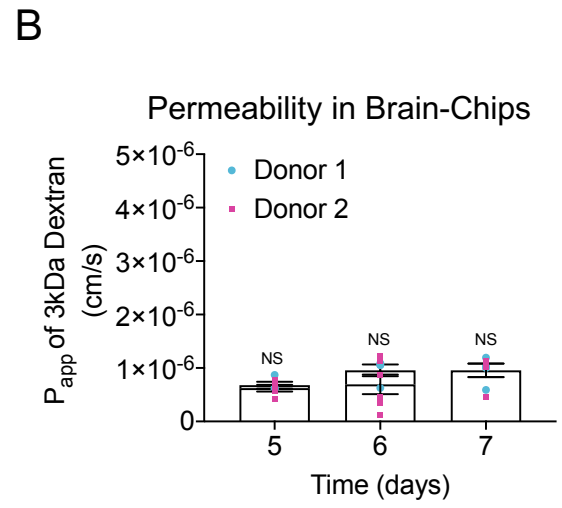
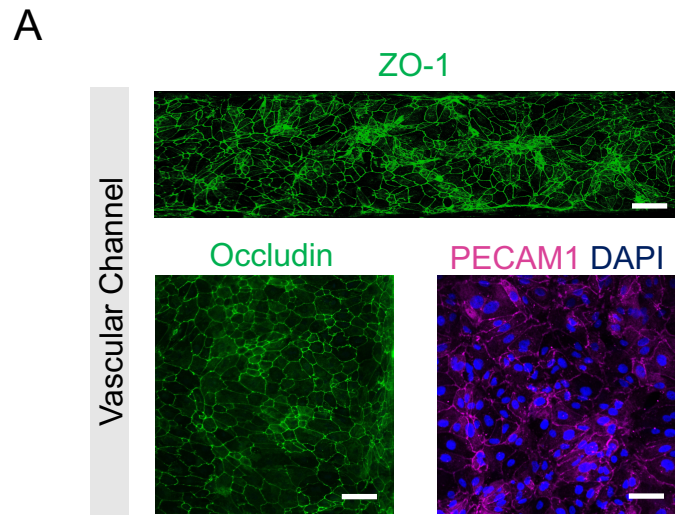


Figure 3

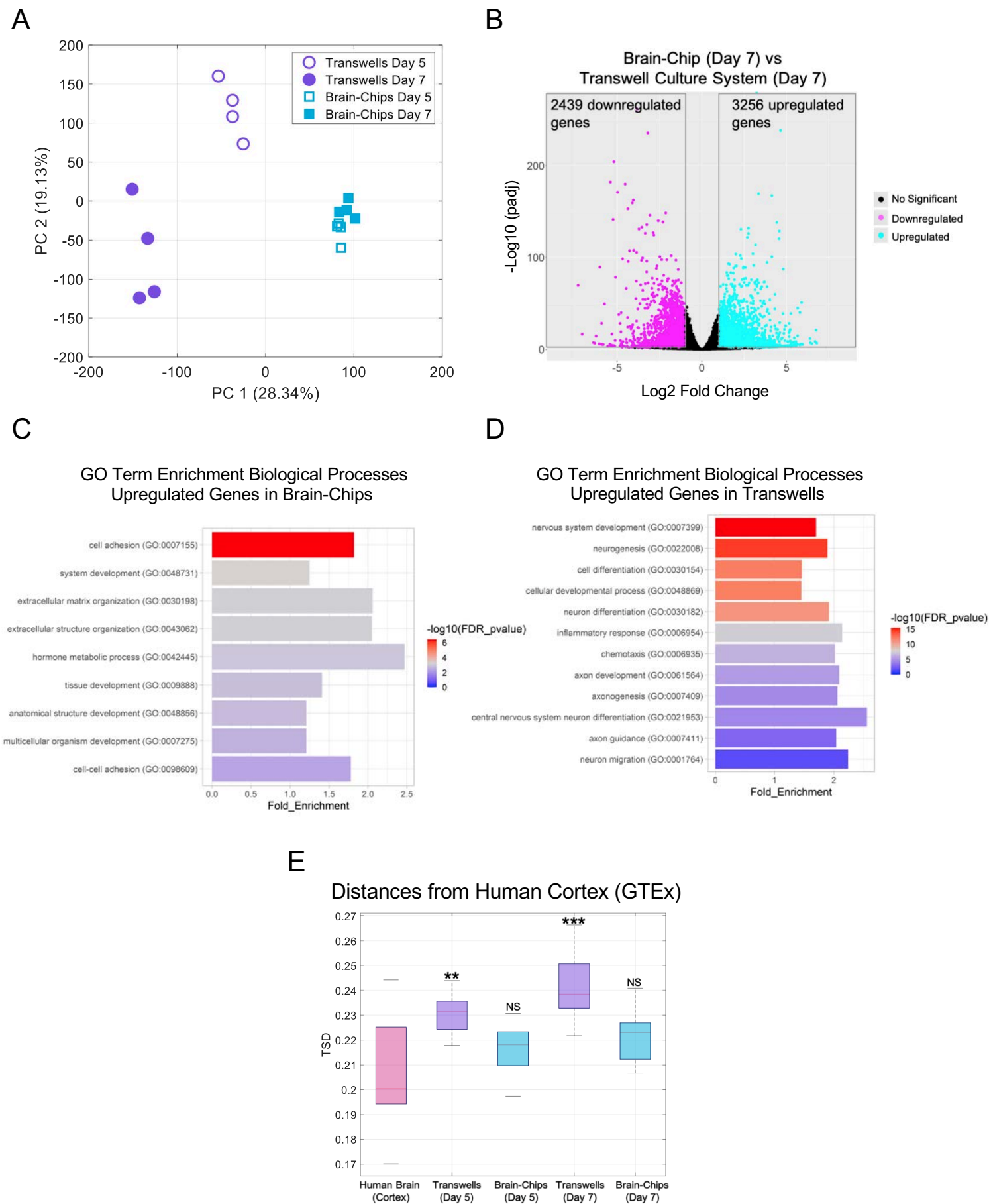


Figure 4

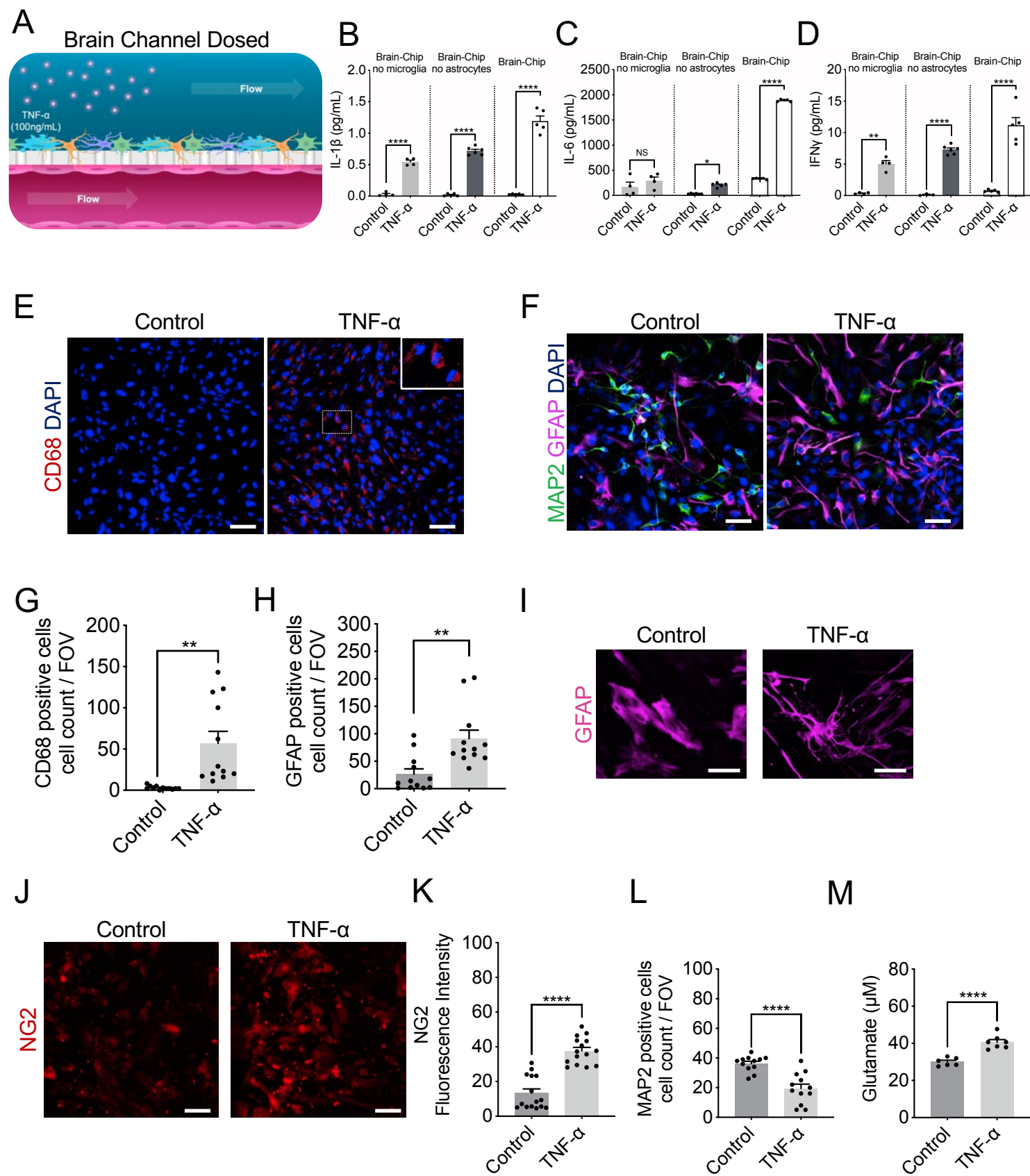
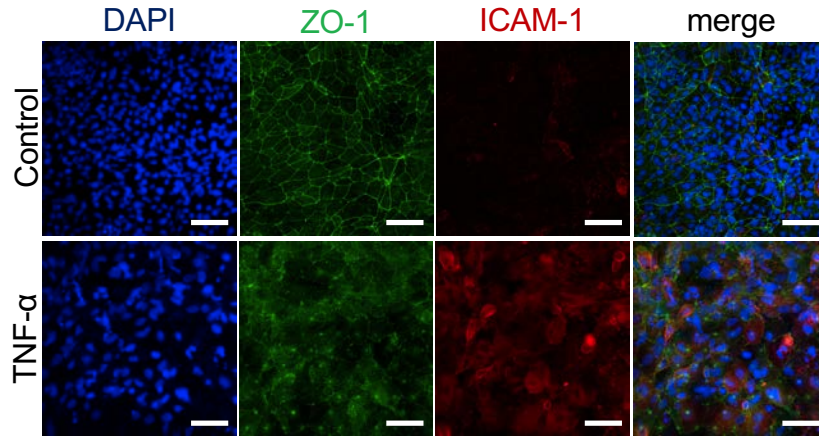
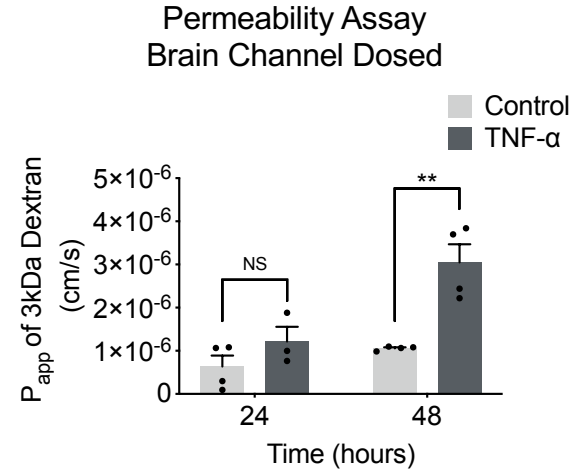


Figure 5

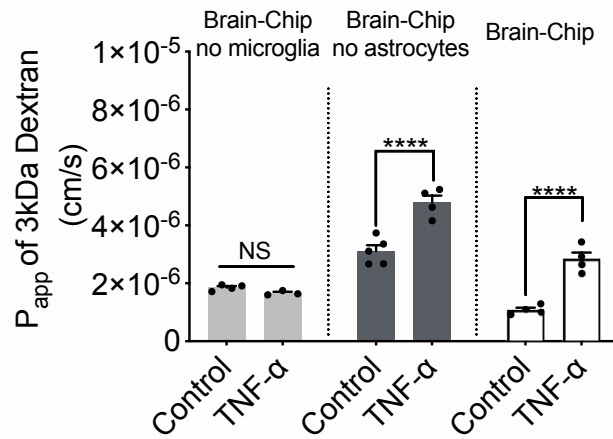
A



B



C



D

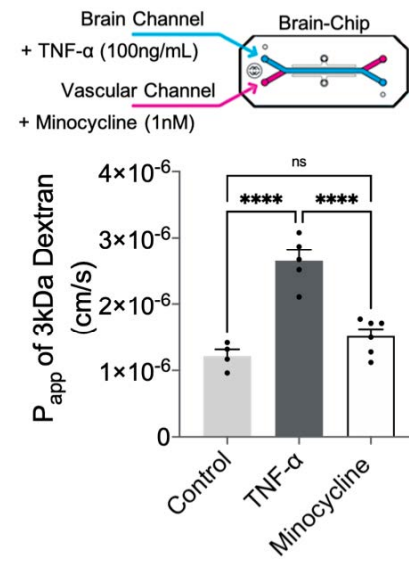


Figure 6

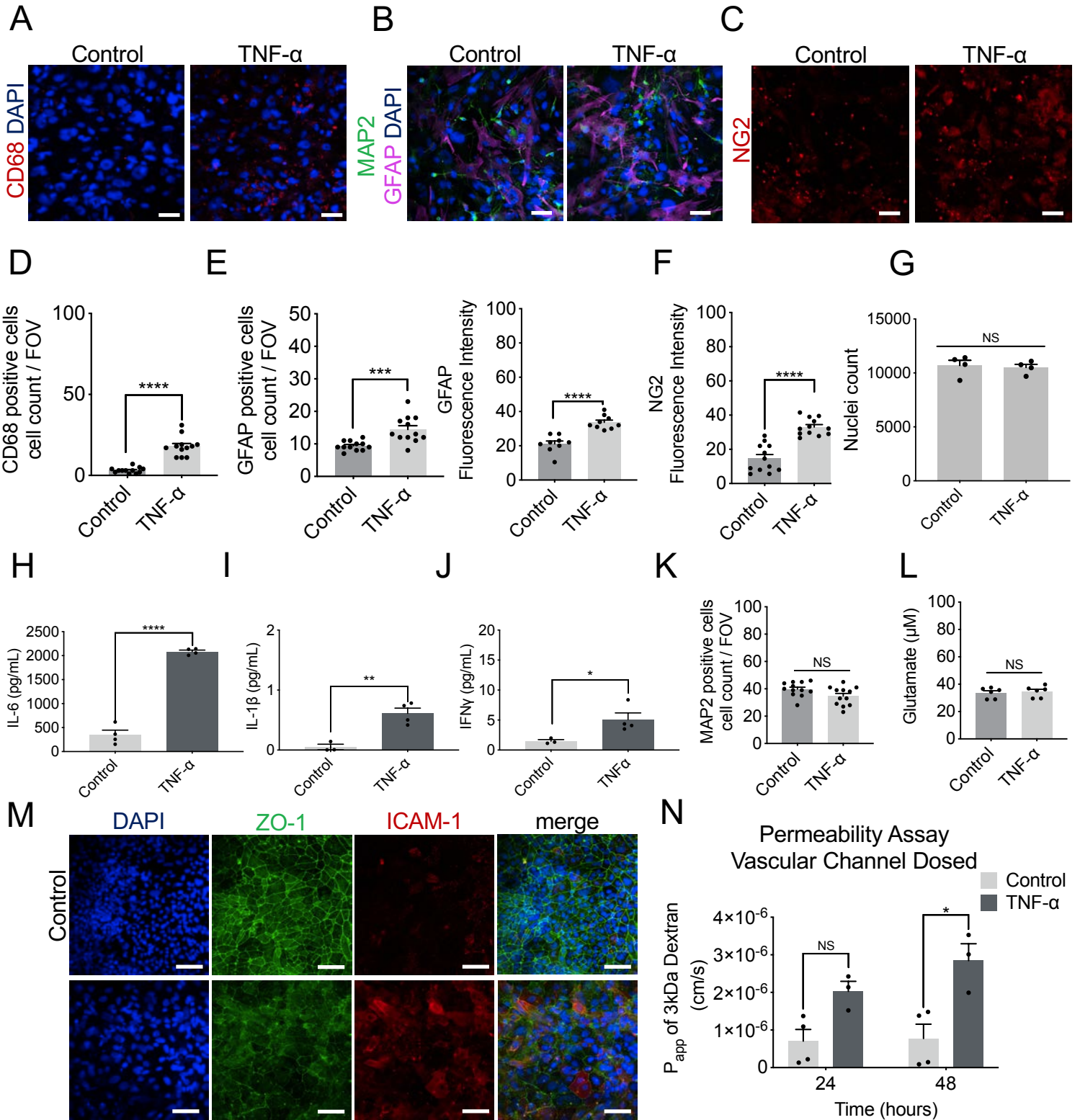


Figure 7

